NUMERICAL SIMULATIONS OF BUBBLE DYNAMICS

Dr. Nikos A. Pelekasis

Assistant Professor of Computational Fluid Dynamics, Dept. Mechanical & Industrial Engineering, University of Thessaly, Volos 38334, GREECE
Tel: 3024210-74102 Fax: 74050, Email: pel@uth.gr

Running title: Numerical Simulations

ABSTRACT
An extensive account of the available numerical methodologies for capturing the dynamic behaviour and interaction of translating and/or oscillating bubbles is provided. Different numerical schemes are classified in three large categories according to the way by which they capture deformation of the interface, as: boundary integral methods where only the bubble's interface is discretized, boundary fitted schemes where the flow field surrounding the bubble is discretized with the interface being identified as one of the coordinate surfaces, and surface tracking schemes where the entire domain both inside and outside the bubble is discretized while the shape of the interface is described via a volume-of-fluid, a level-set or a polynomial function. The boundary integral method provides a better description of the fine details during the last stages of bubble collapse and break-up. The approach via boundary fitted coordinates allows for proper description of the vorticity field around a bubble as well as the formation of eddies behind a translating bubble, over a wide range of Re. Surface tracking techniques can capture severe topological changes in the bubble shape and consequently provide a means to capture the post break-up or post coalescence dynamics. The impact of recent advances in numerical simulations in the understanding of issues of fundamental importance in bubble dynamics, such as monitoring the details of bubble deformation during collapse and identifying the factors determining the mechanism that triggers path instabilities of rising bubbles, is discussed. Recent developments in the area of direct numerical simulations of bubble dynamics are presented.

I. INTRODUCTION

Ever since *Lord Rayleigh* [1] first studied the spontaneous generation and collapse of bubbles in order to explain the damage of propellers of high-speed boats and submarines, research interest in bubble dynamics has grown significantly and presently encompasses a wide spectrum of natural and technical applications. Gas-liquid separation in adsorption towers, two-phase heat exchange and condensation, mixing in chemical reactors, purification of metal alloys by flotation and ship hydrodynamics are just some of the technical fields where bubble dynamics play an important role [2]. There is also growing interest in the dynamics of bubble growth and dissolution in geophysics, in relation to the processes of heat and mass exchange between the oceans and the atmosphere. More recently, there is additional impetus in the field of nonlinear bubble dynamics in the context of single bubble sono-luminescence, which is a phenomenon associated with light emission during collapse of either a cavitating or a laser induced bubble [3]. An important side effect of bubble collapse is the local temperature rise that stimulates formation of active chemical agents and consequently enhances chemical reactivity [4] (sonochemistry). Finally, during the last decade there is an emerging biomedical application of bubbles in the form of contrast agents, which are essentially micron size bubbles that are encapsulated in a lipid polymer or albumin shell. Today, these bubbles are clinically established markers of vascularity and are used for quantitative blood flow and volume measurements, especially in ultrasound echocardiography [5], due to their large backscatter signal in the ultrasound range frequencies. Controlled oscillations and collapse of such bubbles has also recently been used for enhanced drug and gene delivery [6].

It has thus become increasingly important to capture the details of bubble motion and deformation whether this refers to the onset of shape oscillations or to bubble break-up, collapse and the possible formation of satellite bubbles. Since the early theoretical work by *Prosperetti* [7] on the stability of spherosymmetric bubble oscillations a large amount of theoretical studies have been published investigating parametric excitation of shape modes and exploring the importance of resonant mode interaction. The review article by *Feng & Leal* [8] gives a detailed account of the important theoretical findings in this line of research,

and recently *McDougald & Leal* [9,10] conducted a numerical study on the nonlinear inviscid oscillations of a bubble in order to validate the available theories, using spectral and boundary elements.

Since the study of *Blake & Gibson* [11] on bubble collapse next to a solid boundary, where jet formation during collapse was identified as a primary factor for damage, investigation of bubble break-up has been dominated by the boundary element method due to its cost efficiency in capturing complicated shape topologies [11,12]. Bubble behaviour in response to large amplitude perturbations is also very important in sono-luminescence. In particular, a certain degree of sphericity seems to be important for light emission, as it is associated with the formation of a converging shock wave during bubble collapse [13]. While inviscid theory is enough for describing the dynamics of millimetre sized bubbles, for smaller bubbles with equilibrium radius below 100 μm, such as those employed in sonoluminscence and in biological applications, thermal and viscous damping are also expected to play a role in the dynamics [14]. Consequently, there is increasing interest in incorporating the effect of dissipation in the models describing bubble oscillations, primarily viscous dissipation which becomes increasingly dominant for micron sized bubbles, and this is reflected in a number of recent studies. *Boulton-Stone & Blake* [15] included viscous effects in their study of gas bubbles bursting at a free surface, following an earlier numerical study on drop dynamics by *Lundgren & Mansour* [16]. The idea is the same whether one is working with the boundary layer around a drop or a bubble and lies on the fact that, provided there is no massive separation taking place at the surface, one can integrate across the boundary layer and obtain expressions for the vortical part of the pressure and velocity fields solely based on surface properties [7]. More recently, this methodology has been employed in order to capture the detailed dynamics and investigate the existence of universalities during the collapsing stage of an initially elongated bubble [17,18], with or without internal overpressure.

When a bubble undergoes translation, as is normally the case in bubbly flows, for moderate to large values of Re a region of recirculation is expected to form behind the bubble and a uniformly valid integration across the boundary layer can no longer be applied as a means to account for viscous effects. This effect, along with the significantly smaller inertia that characterizes the gas inside the bubble in comparison with the surrounding liquid, are two prominent features of bubbly flows that call for special treatment and indeed they have attracted the attention of researchers in the past decades. A thorough review of the literature in this area of research has been given by *Magnaudet & Eames* [19]. A brief account of the most important results regarding the different forces exerted upon a translating bubble, in relation to the numerical methodology that was used, is provided in the following. Following an earlier theoretical study by *Moore* [20] that provided the drag coefficient of a moving bubble considering the effect of the thin boundary layer and the wake region behind the bubble, *Miksis et al*. [21] used the boundary integral method in order to calculate the steady shape acquired by a rising bubble. In an effort to account for viscous dissipation in the separated region behind the bubble *Ryskin & Leal* [22,23] developed a boundary fitted finite difference method for the solution of steady axisymmetric flow past a deforming bubble. In this fashion they were able to capture similar ellipsoidal and spherical-cap bubble shapes as in [21], but also the structure of separated flow behind a rising bubble. A time dependent boundary fitted numerical scheme, based on the finite volume methodology, was developed by *Takagi et al*. [24] and was applied to the case of axisymmetric flow past a rising bubble in order to verify previously obtained empirical relations for the drag coefficient covering the entire range of Re. A similar methodology was developed by *Magnaudet et al* [25] for calculating the drag, added mass and lift force on bubbles in steady axisymmetric [25] and three dimensional flows [26]. The latter studies aim at validating and extending available

theoretical and/or empirical correlations for the different forces affecting bubble motion. Such correlations find extensive use in simulations of bubbly flows.

This type of research activity is also greatly motivated by the fundamental problem of path instabilities that are often observed in bubbles rising in various kinds of liquids, when the relevant Re exceeds certain threshold values. A central issue in this problem is the role of the wake in the mechanism that triggers the instability, especially since shape oscillations have been experimentally observed as a concomitant phenomenon in occasions where bubbles exhibit a zigzag motion [27] with a frequency that determines the frequency of vortex shedding. Nevertheless, this only happens beyond a critical bubble radius, R_{Cr}=4mm, below which vortex shedding takes place at a frequency that is independent from that of shape oscillations. In a similar experimental study *Wu & Gharib* [28] found that spherical bubbles become unstable and give rise to a zigzagging path whereas when ellipsoidal bubbles become unstable they exhibit a helical trajectory. The basic question underlying the above experimental and theoretical/numerical studies is whether it is the unsteadiness of the wake that triggers the unsteadiness of the bubble's path, as was originally suggested by Saffman [29], or whether it is the unsteadiness of the bubble's shape that determines the behaviour of the wake. A related problem is that of chaotic bubble motion, also known as the 'dancing bubble problem', that arises when the sound amplitude exceeds a certain threshold [30]. Utilizing an old idea by *Saffman* [31] for self propulsion, *Benjamin and Ellis* [32] obtained a formula for the drift velocity of an oscillating bubble as a consequence of second order interaction between two neighboring shape modes, in the context of inviscid theory. Clearly then, bubble drift involves different types of dynamic interaction phenomena, the proper simulation of which has motivated development of quite sophisticated theoretical and numerical techniques in the recent years.

Bubble behaviour in bubbly flows but also single bubble motion involves, especially at large Re or large acoustic disturbances, a wealth of dynamic phenomena some of which entail severe topological changes such as break-up and formation of satellite bubbles or coalescence. Boundary integral techniques or boundary fitted finite difference, finite volume and finite element methods can only capture bubble dynamics, with varying degrees of accuracy, until slightly before a severe topological change takes place. To proceed beyond that point an ad hoc assumption of some sort has to be introduced in the model. As an alternative approach that allows for a smooth transition between different flow topologies different interface tracking methods have been developed, i.e. front-tracking [33], volume of fluid [34] and level set [35] methods, where the entire domain is discretized including the interior of the bubble, and the material properties are advected with the velocity of the interface. Material properties are taken to be constant over each phase while they are assumed to vary across interfacial boundaries via an indicator function that can be as smooth as desired. The location of the interface is monitored by following marker points (front-tracking methods), a volume of fluid function (volume of fluid methods) or a level set function for level set methods. Provided the two phases remain incompressible such methods can give a fairly accurate description of interesting dynamic phenomena such as formation of satellite bubbles or coalescence [36]. This is a rapidly expanding field of research that is expected to evolve into an alternative to experimental observations, especially when control of key physical parameters is difficult to maintain in the laboratory environment, and provide reliable numerical experiments of bubbly flows.

In the next section the equations governing the dynamic behaviour of a bubble in a viscous fluid are outlined and the basic mathematical and numerical principles behind boundary integral, boundary fitted and interface tracking methods are presented. Then, an up to date account of the major results obtained via each of the above methodologies is given, in the context of important physical questions that have attracted the attention of researchers in the

field of bubble dynamics. Finally the current state of the art is reviewed and the advantages and drawbacks of the different methods are discussed, conclusions are drawn and directions for future research are proposed.

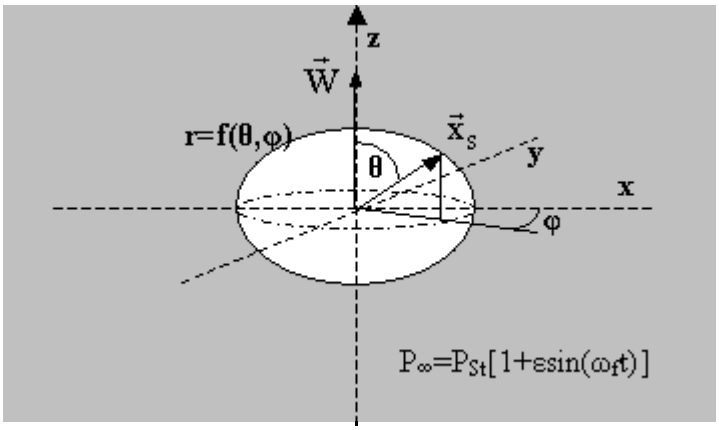

Figure 1: Schematic diagram of a translating bubble that may also subject to acoustic disturbances

II. STATEMENT OF THE GENERAL PROBLEM

The general problem that is of interest here is that of a deforming bubble that may accelerate at the same time owing to some external forcing, e.g. due to gravity or sudden exposure to a shear flow in the far field, or simply perform shape and volume oscillations in response to an acoustic pressure disturbance, Fig. 1. The gas inside the bubble may be considered to be compressible in which case the ideal gas law is a valid assumption for the description of pressure variations inside the bubble

$$P_B(t=0)S_B^{\kappa}(t=0) = P_B(t)S_B^{\kappa}(t) \tag{1}$$

for a bubble performing adiabatic oscillations; κ denotes the polytropic constant, which is normally set to 1.4 for an ideal gas, and S_B the bubble volume. Other types of relations for the pressure vs. volume dependence inside the bubble have been used, however we adopt the adiabatic law for simplicity. The important assumption here is that due to the small gas density pressure is assumed to be uniform inside the bubble, while the shear force exerted on the interface with the surrounding medium vanishes due to the negligible viscosity of the gas. Initially, the bubble is resting at its equilibrium spherical position with equilibrium radius R_0, and the surrounding medium is quiescent with far field pressure P_{St}. Thus, at static equilibrium pressure drop on the bubble's interface is balanced by surface tension,

$$P_B(t=0) - (P_{St} + \rho \mathbf{g}\cdot\mathbf{x}) = \frac{2\sigma}{R_0}, \tag{2}$$

with $\mathbf{x}$ denoting the position vector of a fluid particle, ρ liquid density and σ the interfacial tension; in the following bold faced symbols will denote vectorial quantities. We consider disturbances due to interaction, with an external pressure wave, an external shear or elongational flow, or simply as a result of gravitational forces as is the case with rising bubbles. The case of an initially elongated bubble is also considered, in the context of LASER induced bubbles, by applying a volume preserving initial perturbation of the form,

$$r = f(t=0_+, r, \theta, \phi) = R_0 + \varepsilon Y_n^m(\theta, \phi) \tag{3}$$

on the bubble's interface, where f signifies the instantaneous shape of the interface as a function of the spherical coordinates (r,θ,φ), and $Y_n^m(\theta,\phi)$ the spherical harmonics. When acoustic disturbances are considered the wave-length of the pressure wave is taken to be

much larger than the bubble radius so that we can neglect spatial characteristics of the wave as well as liquid compressibility and consider a disturbance of the form

$$P_\infty = P_{St}\left[1+\varepsilon\sin\left(\omega_f t\right)\right] = P_{St} + P_A\sin\left(\omega_f t\right); \tag{4}$$

ε and ω_f stand for the amplitude and frequency of the disturbance. The bubble's center of mass is allowed to accelerate with an unknown acceleration $\dot{\mathbf{W}}$ while at the same time its interface is deforming. By superposing the opposite acceleration to the equations of motion the bubble is reduced to rest, as far as its translational motion is concerned, and a fictitious field force $-\rho\dot{\mathbf{W}}$ is added to the Navier-Stokes equations that govern the motion of the surrounding fluid. Thus the equations of motion for an incompressible, isothermal fluid that surrounds the bubble read:

continuity: $\nabla\cdot\mathbf{V} = 0$ (5)

momentum: $\dfrac{\partial\mathbf{V}}{\partial t} + \left(\mathbf{V}\cdot\nabla\right)\mathbf{V} = -\dfrac{\nabla P}{\rho} + \mathbf{g} - \dot{\mathbf{W}} + \dfrac{1}{\rho}\nabla\cdot\underline{\underline{\boldsymbol{\tau}}}$ (6)

far field condition: $\mathbf{x}\to\infty \quad \mathbf{V}\to-\mathbf{W}$ (7)

kinematic condition at the interface in Lagrangian form: $\dfrac{D\mathbf{x}_S}{Dt} = \mathbf{V}_S$ (8)

dynamic condition: $\mathbf{x}=\mathbf{x}_S: \quad -P_B\mathbf{n} - \left(-P\underline{\underline{\mathbf{I}}} + \underline{\underline{\boldsymbol{\tau}}}\right)\cdot\mathbf{n} = 2\sigma H\mathbf{n} = \sigma\left(-\nabla_S\cdot\mathbf{n}\right)\mathbf{n},$ (9)

where $\mathbf{n}$ denotes the outwards pointing unit normal vector with respect to the fluid surrounding the bubble, ρ, μ, the density and viscosity of the fluid, ∇_s, H, the surface gradient and mean curvature on the bubble's interface, respectively, and $\underline{\underline{\mathbf{I}}}$, $\underline{\underline{\boldsymbol{\tau}}} = \mu\left(\dfrac{\partial V_i}{\partial x_j} + \dfrac{\partial V_j}{\partial x_i}\right)$, the unit and deviatoric stress tensor, respectively. Finally, the instantaneous velocity, $\mathbf{W}$, of the center of mass of the bubble is obtained by the force balance,

$$0 = \rho_B S_B\mathbf{g} - \rho_B S_B\dot{\mathbf{W}} + \oiint_A\left(-P\underline{\underline{\mathbf{I}}} + \underline{\underline{\boldsymbol{\tau}}}\right)\cdot\left(-\mathbf{n}\right)dA\,. \tag{10}$$

If a solid boundary is present, or when the bubble interacts with an external shear flow the no slip boundary condition and the appropriate far field condition [26] are used, with the understanding that for a steady flow $\dot{\mathbf{W}} = 0$;

$$\mathbf{V} = 0, \text{ for a solid surface and } \mathbf{V} = \left(W+\alpha y\right)\mathbf{e}_Z \text{ for an external shear flow} \tag{11}$$

Since the density of the bubble is negligible in comparison with that of the surrounding fluid the first two terms in Eq. (10) are normally dropped. If a characteristic velocity U is chosen then, along with equilibrium bubble radius R_0 that is used as a characteristic length, time, space, velocity and pressure are rendered dimensionless and the following dimensionless parameters that determine the bubble motion, arise:

$$\mathrm{Re} = \frac{\rho U R_0}{\mu}, \quad \mathrm{We} = \frac{\rho U^2 R_0}{\sigma}, \quad \mathrm{Bo} = \frac{gR_0}{U^2}, \quad \mathrm{Sh} = \frac{R_0\alpha}{U}, \quad P_D = \frac{P_{St}}{\rho U^2}, \quad \varepsilon, \quad \omega = \frac{\omega_f R_0}{U} \tag{12}$$

The first four parameters are identified as the Reynolds, Weber, Bond and Shear numbers whereas the last three define the dimensionless pressure datum the amplitude and the frequency necessary for the description of an acoustic disturbance; $\mathbf{e}_Z$ is the axis that is aligned with gravity. Each one of the four dimensionless numbers represents the relative importance of the different forces that affect the dynamic behaviour of the bubble. Depending on the specific problem under investigation U is determined via the inertia, surface tension, gravitational, shear or acoustic forces and this eliminates one of the above parameters riving rise to the appropriate system description. In the problems of interest to bubble dynamics

viscous forces are normally small and consequently 1/Re is a small quantity that is either dropped, if the potential flow assumption is employed, or remains in the problem as a parameter that is often amenable to simplifying asymptotic analysis. When bubble-bubble, bubble- interface or bubble –rigid boundary interactions are studied an additional parameter arises, namely the ratio $\gamma=h/R_0$ between the initial distance and the bubble's equilibrium radius.

III. DESCRIPTION OF THE MAJOR NUMERICAL METHODOLOGIES

Based on the above description the numerical problem consists of calculating the velocity and pressure fields in the surrounding medium along with the shape of the interface and the bubble velocity as a function of time and space. It is a complicated dynamic problem that warrants special attention. An outline of the available numerical methodologies is provided in the following.

III.1 Boundary Integral Method

When the flow around the bubble is characterized by large Re and, in case of rectilinear motion of the center of mass of the bubble, the wake effects are not very important, the assumption of irrotationality in the surrounding liquid holds and the velocity field is essentially described by the Laplacian [37]:

$$\mathbf{V}=\nabla\Phi,\quad \nabla^2\Phi=0. \tag{13}$$

Then, the pressure variation in the liquid is given by the dynamic version of Bernoulli's law,

$$\frac{\mathrm{D}\Phi}{\mathrm{D}t}-\frac{1}{2}\left[\left(\frac{\partial\Phi}{\partial n}\right)^2+\left(\frac{\partial\Phi}{\partial s}\right)^2\right]+\mathrm{P}+\mathrm{Bo}\mathbf{e}_Z\cdot\mathbf{x}+\dot{\mathbf{W}}\cdot\mathbf{x}=\mathrm{P}_\mathrm{D}\left[1+\varepsilon\sin(\omega t)\right]+\frac{1}{2}|\mathbf{W}|^2 \tag{14}$$

in dimensionless form; n and s denote coordinates that vary along the bubble's surface and normal to it, respectively, for an axisymmetric bubble. When the problem of a rising bubble is studied, $\mathbf{g}=-g\mathbf{e}_Z$, $\mathbf{W}=W\mathbf{e}_Z$, and in the above equation the gravitational and acceleration terms assume the form $\left(\mathrm{Bo}+\dot{W}\right)z$. In the same context, the velocity potential in the far field becomes,

$$\Phi=-Wz \tag{15}$$

whereas at the bubble's interface the kinematic condition for a free surface is applied:

$$\frac{\mathrm{D}\mathbf{x}_S}{\mathrm{D}t}=\mathbf{V}_S=\nabla\Phi \tag{16}$$

The Lagrangian representation is adopted here so that interfacial shapes that are not single-valued in the Eulerian frame can also be captured,

$$\frac{\mathrm{D}}{\mathrm{D}t}=\frac{\partial}{\partial t}+\mathbf{V}\cdot\nabla. \tag{17}$$

The problem description is completed with the imposition of the adiabatic law, Eq. (1), inside the bubble, the normal force balance at the interface,

$$\mathrm{P}_B-\mathrm{P}=-\frac{1}{We}2H=\frac{1}{We}\nabla_S\cdot\mathbf{n}, \tag{18}$$

where –2H is the mean curvature of the bubble's surface, and the force balance determining the rectilinear motion of the bubble, i.e. Eq. (10).

The latter balance is only used when weak viscous effects are included in the model describing a bubble rising in a quiescent fluid in which case the evolution of its rectilinear velocity $\mathbf{W}$ can be obtained as part of the numerical solution. To this end the pressure and velocity fields are decomposed as suggested in [38] in a rotational and an irrotational part

$$\mathbf{V}=\mathbf{u}+\mathbf{U},\quad \mathrm{P}=\mathrm{p}+\Pi \tag{19}$$

where lower case symbols denote irrotational quantities. It can be seen that the rotational velocity field can be described via a vector potential which, due to axisymmetry, is of the form,

$$\mathbf{U} = \nabla \times \mathbf{A}, \quad \mathbf{A} = \mathrm{A}\left(\mathrm{r},\theta\right)\mathbf{e}_{\phi} \tag{20}$$

with $\mathbf{e}_{\phi}$ denoting the azimuthal unit vector. Now the tangential condition on the bubble's interface can also be imposed,

$$\mathbf{t}\cdot\left[\nabla\mathbf{V}+\nabla\mathbf{V}^{\dagger}\right]\cdot\mathbf{n}=0\,. \tag{21}$$

where $\vec{t}$ signifies the unit vector tangential to the interface. Combining the requirement for zero shear on the interface with that for continuity the appropriate scales for the tangential and normal components of $\mathbf{U}$ can be obtained, $n \sim \delta$, $U_t \sim \delta$, $U_n \sim \delta^2$, $A \sim \delta$, $\Pi \sim \delta$, where δ is the size of the boundary layer. Substituting in the momentum equation an estimate for $\delta \sim Re^{-1/2}$ is provided and subsequent integration across the boundary layer eliminates unwanted normal derivatives [15,16,17]. Substituting the weak viscous correction in the normal force balance we get a revised form of Eq. (14) for the evolution of the velocity potential in terms of quantities evaluated on the interface:

$$\frac{d\Phi}{dt}=\frac{1}{2}u^2+u_n U_n+P_{\infty}-P_B-2H-\left(Bo+\dot{W}\right)z+\Pi+\frac{1}{2}\left|\mathbf{W}\right|^2-\frac{2}{Re}\left(\mathbf{n}\cdot\nabla\mathbf{u}\cdot\mathbf{n}\right) \tag{22}$$

There is still one remaining quantity to be evaluated, namely the rising velocity of the bubble, which arises as an additional unknown in a dynamic calculation. This can be done in a consistent manner by satisfying an integral form of Eq. (22) that corresponds to the axial component, i.e. the one in the direction of gravity, of the force balance on the bubble:

$$\int_0^{\pi}\left[\frac{d\Phi}{dt}-\frac{1}{2}u^2-u_n U_n+\left(Bo+\dot{W}\right)z-\Pi+\frac{2}{Re}\left(\mathbf{n}\cdot\nabla\mathbf{u}\cdot\mathbf{n}\right)\right]\left(\mathbf{e}_Z\cdot\mathbf{n}\right)ds \tag{23}$$

The final step of this formulation is related to the evaluation of the normal derivative of the potential on the bubble's surface based on the potential itself on the bubble as well as on the rest of the boundaries. This is done by substituting for the Laplacian an integral equation that relates the potential to its normal derivative, through Green's theorem. To this end, we apply Green's third identity on the axially symmetric Green's function of the Laplacian and the quantity $\Psi = \Phi + Wz$, where the term Wz arises in the context of a translating bubble.

$$\Psi\left(\hat{r},\hat{\theta},t\right)+\int_0^1\left[\Psi\left(r,\theta,t\right)-\Psi\left(\hat{r},\hat{\theta},t\right)\right]\frac{\partial G}{\partial n}\left(\hat{r},\hat{\theta},r,\theta\right)r\sin\theta\left(r_{\xi}^2+r^2\theta_{\xi}^2\right)^{1/2}d\xi = \int_0^1\frac{\partial\Psi}{\partial n}G\left(\hat{r},\hat{\theta},r,\theta\right)r\sin\theta\left(r_{\xi}^2+r^2\theta_{\xi}^2\right)^{1/2}d\xi, \tag{24}$$

where, $z\left(r,\theta\right)=r\cos\theta$ is the appropriate form of the axial coordinate when the center of mass of the bubble is used as the origin. When the bubble interacts with a free surface or with another bubble another two integrals arise in eq. (24) involving the potential and the flux on the interacting surface. Application of the appropriate dynamic and kinematic conditions at the additional interface completes the formulation [11, 41]. The specific form of the integral on the left hand side of Eq. (24) is used in order to regularize the strong singularity in the normal derivative of the Green's function [39]. The great advantage of the above formulation lies in the fact that only the interface needs to be discretized rather than the entire space, while the far field boundary condition is inherently satisfied as a result of the form of the singular kernels that are used. Consequently when axisymmetry is assumed only the generating curve of the bubble's surface has to be discretized and the whole problem is treated as a PDE with Φ, A, r and θ as functions of time and of the location of the specific particles that are followed in the Lagrangian reference frame.

Typically, the description of the unknown functions is provided in terms of a sum of basis functions in the finite element fashion, hence this approach is also known as the boundary element method [40]. B-cubic splines are often employed as basis functions owing to their favorable accuracy and smoothness characteristics, continuity up to the second derivative, that guarantee accurate description of complicated topologies [9,10,41,42]. The method can be extended to three dimensional flow arrangements as long as large Reynolds numbers are involved. When $\mathbf{W} = 0$ and capillary forces are used for the velocity scale, $U=(\sigma/\rho/R_0)^{1/2}$, the case of free bubble oscillations is examined, whereas when acoustic forces are used for the velocity scale, $U=\omega_f R_0$, the case of a cavitating bubble is examined. Finally, when a non-vanishing acceleration $\dot{\mathbf{W}}$ is assumed and gravity is used for rendering velocity dimensionless, $U=(gR_0)^{1/2}$, the problem of a rising bubble is addressed [21]. Some important findings regarding these problems, obtained via the boundary integral methodology, will be presented in the next section.

III.2 Boundary Fitted Coordinate Systems

This approach is adopted when the Reynolds number describing the flow around the bubble is moderate, in which case the full Navier-Stokes equations have to be employed in order to capture the characteristics of the motion. This is especially true in the case of rising bubbles where the structure of the wake is of interest and the effect it has on the drag and lift coefficients and on the destabilizing mechanism that leads to deviations from the rectilinear path has been the subject of a large number of research efforts in the past two decades. The basic idea lies in the fact that, given the shape of the boundary, mapping functions can be obtained, $r(\xi,\eta)$ & $z(\xi,\eta)$ where r,z,φ, denote the coordinates of the cylindrical coordinate system with z the direction of the axis of symmetry, such that the transformed coordinates $(\xi,\eta)\in[(0,1),(0,1)]$ and r, z satisfy the covariant Laplace equations

$$\frac{\partial}{\partial\xi}\left(f\frac{\partial z}{\partial\xi}\right)+\frac{\partial}{\partial\eta}\left(\frac{1}{f}\frac{\partial z}{\partial\eta}\right)=0,\qquad h_\xi=\sqrt{\frac{\partial^2\rho}{\partial\xi^2}+\frac{\partial^2 z}{\partial\xi^2}}, \tag{25}$$

$$\frac{\partial}{\partial\xi}\left(f\frac{\partial\rho}{\partial\xi}\right)+\frac{\partial}{\partial\eta}\left(\frac{1}{f}\frac{\partial\rho}{\partial\eta}\right)=0,\qquad h_\eta=\sqrt{\frac{\partial^2\rho}{\partial\eta^2}+\frac{\partial^2 z}{\partial\eta^2}}\,. \tag{26}$$

In the above, $f(\xi,\eta)$ is the so called distortion function that represents the ratio between the metrics along the two transformed coordinates, $f(\xi,\eta)=h_\eta/h_\xi$. It is well known that solutions of the Laplacian constitute orthogonal transformations. Consequently, given the boundary shape and provided the mapping functions for z and r satisfy appropriate boundary conditions, the boundary surface becomes a coordinate surface in the transformed domain. Thus, the entire domain is described via the transformed coordinates that are orthogonal by construction, with f controlling the density of the coordinate lines [22]. If the shape of the boundary is simple, as is the case with a spherical bubble, known expressions from conformal mapping can be used as in [25], where $\xi=\Phi$, $\eta=\Psi$, with Φ and Ψ denoting the potential and stream function, respectively. Subsequently, the equations of motion and continuity [25] or the equations describing variations of vorticity and stream function [22] are expressed in the transformed coordinates. The formulation in terms of the primitive variables is given herein, following [25, 43], in compact conservative form for continuity and momentum,

$$\sum_j \nabla\cdot_j V_j=0,\qquad H_i^j=\frac{1}{h_i}\frac{\partial h_i}{\partial\xi_j},\qquad \nabla_i(\ )=\frac{\partial(\ )}{\partial\xi_i}+\sum_{k\neq i}H_i^k(\ ) \tag{27}$$

$$\frac{\partial V_i}{\partial t}+\sum_j\nabla\cdot_j\left(V_iV_j-\frac{1}{Re}\tau_{ij}\right)=-\frac{1}{h_i}\frac{\partial P}{\partial\xi_i}-\sum_j H_i^j\left(V_jV_i-\frac{1}{Re}\tau_{ji}\right)+\sum_j H_j^i\left(V_jV_j-\frac{1}{Re}\tau_{jj}\right). \tag{28}$$

Next, the equations are discretized in the spatial dimensions in various ways, e.g. the finite difference [22,23] and the finite volume [25] approaches have been extensively used in the past with success, along with the appropriate time integration scheme. Besides the standard far field and symmetry conditions employed for axisymmetric flows, special care is needed for the outflow conditions in regions where the flow leaves the computational domain. To this end a set of parabolic approximations is imposed on the flow field right at the boundary where it leaves the domain (n, s signify the normal and tangential directions with respect to the boundary) [25],

$$\frac{\partial^2 V_N}{\partial n^2}=0,\quad \frac{\partial^2 V_t}{\partial n}=0,\quad \frac{\partial^2 P}{\partial n \partial s}=0. \tag{29}$$

Due to difficulties encountered in the existence and uniqueness of the mapping generation schemes [44] a quasi-conformal mapping technique was introduced by *Duraiswami & Prosperetti* [45] for the appropriate generation of orthogonal meshes in single or even multiply connected domains, that utilizes the boundary integral method for the solution of the Laplacian and adds flexibility in the imposition of the boundary conditions. This approach has been independently proposed by *Kang & Leal* [46] and has been widely adopted ever since [47] for flows around curved free surfaces. Nevertheless, when highly curved surfaces are involved there is still some discrepancy in the numerical results regarding the formation of standing eddies behind a translating bubble with an intensely oblate axisymmetric shape [47,48], which attests to the difficulty in capturing the behaviour of the wake for such flows and to their possible susceptibility to three dimensional disturbances [47].

In the finite element literature regarding flows with a free surface both algebraic and Elliptic mesh generation schemes have been employed. The former approach typically amounts to transforming the coordinate system in such a way that the boundary surfaces become coordinate lines, e.g. in the case of an oscillating bubble a transformation of he form $\eta=r/f(\theta,t)$, with $\eta\in(1,\infty)$ and $r=f(\theta,t)$ the location of the interface, would be such an algebraic transformation; r, θ denote the appropriate spherical coordinates for axisymmetric domains. The transformed flow domain is discretized by elements that are bordered by fixed spines and by a set of curves that move proportionally to the free surface along the spines. In axisymmetric domains the spines are normally lines of constant θ [49,50]. Despite the fact that algebraic schemes give rise to non-orthogonal meshes, they tend to be computationally efficient. But, they require a significant amount of user interaction to define workable meshes. Moreover, this type of mesh generation may lead to excessive distortion and, sometimes, even crossing of the coordinate surfaces. Similar issues arise when conformal mapping is used in order to produce orthogonal meshes out of highly distorted interfaces.

The basic principles for optimal mesh generation were laid out by *Salzman & Brackbill* [51]. It evolves around three important criteria, namely orthogonality, smoothness and density of coordinate lines in regions where large variations occur. Algebraic meshing can accommodate the third criterion only. Elliptic mesh generation, via solution of a partial differential equation for each computational coordinate, has been exploited extensively in order to satisfy orthogonality. In the finite element literature, a significant amount of research has gone into accommodating a combination of the above criteria. In particular, *Christodoulou & Scriven* (1992) [52] introduced the generalized Cauchy-Riemann conditions,

$$S\xi_x=\eta_y,\quad S\xi_y=-\eta_x, \tag{30}$$

in association with the orthogonality functional,

$$I_O=\iint_D\left[\left(\sqrt{S}\xi_x-\frac{1}{\sqrt{S}}\eta_y\right)^2+\left(\sqrt{S}\xi_y+\frac{1}{\sqrt{S}}\eta_x\right)^2\right]dxdy \tag{31}$$

for two dimensional problems; x, y, signify Cartesian coordinates. The Euler-Lagrange equations corresponding to this functional are,

$$\nabla\cdot\left(S\nabla\xi\right)=0,\quad \nabla\cdot\left(\frac{1}{S}\nabla\eta\right)=0,\quad S=\sqrt{\frac{x_\xi^2+y_\xi^2}{x_\eta^2+y_\eta^2}}\,. \tag{32}$$

On the basis of this orthogonality functional the above investigators proposed the following mapping equations,

$$\nabla\cdot\left[\sqrt{\frac{x_\xi^2+y_\xi^2}{x_\eta^2+y_\eta^2}}+\varepsilon\right]\nabla\xi+\frac{\varepsilon_1}{J}\frac{\partial}{\partial\xi}\ln\left[\left(x_\xi^2+y_\xi^2\right)f\left(\xi\right)\right]=0,\qquad J=x_\xi y_\eta-x_\eta y_\xi, \tag{33a}$$

$$\nabla\cdot\left[\sqrt{\frac{x_\eta^2+y_\eta^2}{x_\xi^2+y_\xi^2}}+\varepsilon\right]\nabla\eta+\frac{\varepsilon_2}{J}\frac{\partial}{\partial\eta}\ln\left[\left(x_\eta^2+y_\eta^2\right)g\left(\eta\right)\right]=0\,, \tag{33b}$$

where ε weighs the smoothness functional measure

$$I_S=\iint_D\left[\left(\nabla\xi\right)^2+\left(\nabla\eta\right)^2\right]dxdy \tag{34}$$

relative to the orthogonality functional measure I_O, and ε_1, ε_2 control the concentration of the mesh in the ξ and η direction, respectively. The first two terms in (33a) and (33b) are the result of minimizing the functional $I_O+\varepsilon I_S$ and the third term is added in order to control the spacing of the mesh. In the ensuing years variations of the above approach have been presented, for two dimensional and axisymmetric geometries, based on the idea that the role of the two coordinate lines is different. The coordinate lines parallel to the surface (ξ curves) should follow or even concentrate close to the interface, while the coordinate lines normal to the interface (η curves) are simply required to intersect smoothly and orthogonally with ξ curves [53,54]. Most notably, ε_2 was set to zero for the η lines and their concentration was basically controlled by the imposed boundary conditions. Whenever required parameters ε, ε_1 and ε_2 are chosen so that ellipticity of the equations is retained. This quasi-elliptic approach has not found extensive use in the field of bubble dynamics but it has some very promising features.

III.3 Surface Tracking Methods

With the term surface tracking methods we refer to a class of numerical schemes dedicated to the simulation of two-phase flows where severe topological changes may occur. In this methodology a Eulerian grid is employed for the discretization of the entire domain, which in our case consists of the gas and the liquid phase. In most schemes available in the literature both phases are taken to be incompressible. There have been surface tracking schemes in the literature that deal with different equations of state for different fluids, and consequently can handle compressibility [55], but standard practice is to assume incompressibility throughout the computational domain. As a first step in this approach surface tension forces are incorporated in the Navier-Stokes equations in the form of a volume force [56], $\sigma\left(-2H\right)\nabla I$, where (-2H) is the mean curvature and I the Heaviside function that equals unity in one of the two phases and vanishes in the other one. The numerical feature that characterizes different surface tracking methods is the fashion by which the instantaneous location of the interface is calculated. Depending on the method,

- An indicator function is introduced that is a field function, $I=I\left(\mathbf{x}\right)$, when the front tracking (FT) approach is employed [33], it is constant within each fluid and has a finite transition zone up to grid points nearest to the interface. It is utilized in calculating the material properties,

$$\rho(\mathbf{x}) = \rho_0 + (\rho_b - \rho_0) I(\mathbf{x}), \quad \mu(\mathbf{x}) = \mu_0 + (\mu_b - \mu_0) I(\mathbf{x}), \tag{35}$$

and it is evaluated, once the interface location is known, via solution of the Laplacian. Essentially it is calculated through a distribution function $D(\mathbf{x} - \mathbf{x}_S)$ that determines what fraction of an interface property should go to each grid point. This requires a separate moving grid for tracking the position of the interface marker points via their velocity, $\mathbf{u}_S^i$

$$\frac{d\mathbf{x}_S^i}{dt} = \mathbf{u}_S^i, \qquad \mathbf{u}_S^i = \sum_j D(\mathbf{x} - \mathbf{x}_S^i)\mathbf{u}_j \tag{36}$$

which in its turn is evaluated by averaging the velocities of the stationary grid points in the vicinity of the interface point. To account for depletion or accumulation of particles in certain areas of the domain computational elements are removed or added accordingly. For calculating properties of the interface, such as the curvature, polynomial approximations are used, once particle connectivity is established by averaging the vector product of the various tangent vectors of neighboring interface grid points.

- Once the mesh is defined each grid cell is associated with a volume of fluid (VOF) function [34] that acquires the following values,

$$f(x,y,t) \equiv \begin{cases} 1 & \text{if there is liquid at point (x,y)} \\ 0 & \text{if there is gas at point (x,y)} \\ & \text{between 0 and 1 at the interface} \end{cases}. \tag{37}$$

Since the type of fluid does not change along path-lines the function f is passively advected with the flow which, in conjunction with continuity, gives the conservation law for f

$$\frac{\partial f}{\partial t} + \frac{\partial (uf)}{\partial x} + \frac{\partial (uf)}{\partial y} = 0 \tag{38}$$

in a two-dimensional flow domain. Based on the above equation, if one uses a conservative finite difference scheme, volume is conserved. The manner in which Eq. (38) is solved numerically is a central issue in VOF schemes. Firstly, the interface has to be reconstructed for given values of f. To this end, a linear approximation to the interfacial shape is produced in multifluid cells, i.e., each cell for which $0 < f(\mathbf{x},t) < 1$, and the normal vector is obtained. Subsequently, the dependent variables in the flow domain are advected by either a fractional step or a second order unsplit advection algorithm [56] and the density and dynamic viscosity are reconstructed by volume weighting,

$$\rho = f(\mathbf{x})\rho_o + \left[1 - f(\mathbf{x},t)\right]\rho_b, \quad \mu = f(\mathbf{x})\mu_o + \left[1 - f(\mathbf{x},t)\right]\mu_b, \tag{39}$$

- A smooth function, $\phi(\mathbf{x},t)$, called the level set function is introduced in the level set (LS) method [57]. Liquid regions are those in which $\phi(\mathbf{x},t) > 0$ while the opposite is true for gas regions. The free surface is implicitly represented by the set of points in which $\phi(\mathbf{x},t) = 0$. The level set function is maintained as the signed distance to the free surface; $\phi(\vec{x},t) = -d$ in the gas and $\phi(\mathbf{x},t) = d$ in the liquid, where d=d(t) is the shortest distance from the point $\vec{x}$ to the free surface at time t [57]. One of the advantages of the LS method is the relatively simple calculation of the curvature of the interface based on the above representation, $-2H = \nabla \cdot \frac{\nabla\phi}{|\nabla\phi|} = \nabla \cdot \mathbf{n}$. For incompressible fluids the level set function obeys the conservation law,

$$\frac{\partial \phi}{\partial t}+\frac{\partial (u\phi)}{\partial x}+\frac{\partial (u\phi)}{\partial y}=0\,. \qquad (40)$$

After the advection process is completed the material properties are obtained by monitoring the level set function. The interface is modeled as having a small but finite thickness for increased smoothness of the results, as was also the case with the FT method. Finally the velocity and pressure fields are obtained via a projection method by appropriate splitting of the Navier-Stokes equations. A typical drawback of the LS method is the loss of mass owing to the nature of the level set function

In order to circumvent problems associated with loss of mass in the LS method, and avoid difficulties encountered in calculating the geometrical characteristics of the interface when the FT and VOF approaches are adopted, hybrid methods have been introduced. One such method is the combined level set and volume of fluid method (CLSVOF) that has been developed [35] for 3D and axisymmetric computations of two-phase flows with quite impressive results [36].

IV. PRESENTATION OF RESULTS FROM NUMERICAL SIMULATIONS

The rapid improvement of computing power that has taken place during the past decades has stimulated a large number of numerical investigations in the field of bubble dynamics. New methods have emerged while older methods have seen significant improvement. Consequently, there has been such an enormous amount of research that has accumulated only in the past few years that makes the task of selecting and presenting the most important results seem almost insurmountable. Nevertheless, an effort will be made to compile the findings of a number of important investigations in the light of some central issues in the field. Such central issues that, in the author's mind, either received satisfying answers via a numerical approach in the past few years or deserve special attention in the future, based on the current state of the art, are: (a) capturing the fine details of bubble instabilities until the last stages of break-up and collapse, (b) identifying the exact role of shape oscillations and the structure of the wake behind a translating bubble in triggering path instabilities and (c) conducting realistic numerical experiments of bubbles that undergo shape oscillations along with a rectilinear motion. These topics are carefully selected because, besides their fundamental importance, they best illustrate the capabilities of the three dominant numerical methods in the field of bubble dynamics.

IV.1 Bubble oscillations, shape instabilities and break-up

One of the first issues that were addressed numerically in the field of bubble dynamics was the mechanism of bubble collapse near solid or free boundaries and the assessment of their destructive power in the context of cavitation damage. It was the pioneering work of *Blake & Gibson* [11] and *Blake et al*. [58], using the boundary integral method, that first identified the effect of jet formation in bubble break-up next to a free boundary or a rigid wall. In the former case an accelerating liquid jet is formed inside the bubble that moves away from the free surface and hits the opposite bubble wall, while a pronounced spike is formed in the free surface that moves away from the bubble jet, Fig 2a. When bubble interaction with a solid wall is considered the liquid jet that is formed inside the bubble is directed towards or away from the wall depending on the ratio γ between, the initial distance from the bubble's center of mass to the free surface and the bubble maximum radius, Figs 2b,2c. These findings have been experimentally [11, 60] verified and instigated scientific interest in jet formation and impact. More recently intensified CCD camera recordings have shown that most of the cavitation damage occurs peripherally around the point where the bubble collapses near the solid surface, as a result of the interaction between the jet and the shock wave that is formed

after collapse [60]. This has stimulated further research on the details of bubble collapse and jet formation. It is known that after collapse the bubble rebounds to a larger radius, which is overpredicted by numerical simulations [59]. As a result the issue of introducing damping mechanisms in the bubble model was raised. Indeed this issue was addressed by means of a front tracking technique [61] that focused on the effect of viscous dissipation. It was seen that jet impact velocity was decreased as viscosity increases whereas impact is impossible below a certain threshold value for Re. Nevertheless, bubble rebound shapes obtained when collapse takes place are very similar to those predicted by the boundary integral method. Finally, the importance of liquid compressibility in refining collapse dynamics and shock formation is stressed. More recently 3D extensions of the boundary element methodology have been developed [62] for the simulation of the interaction between a growing bubble, possibly due to an underwater explosion, and a free floating or rigid structure, with very good agreement with experimental measurements of bubble shapes ant periods.

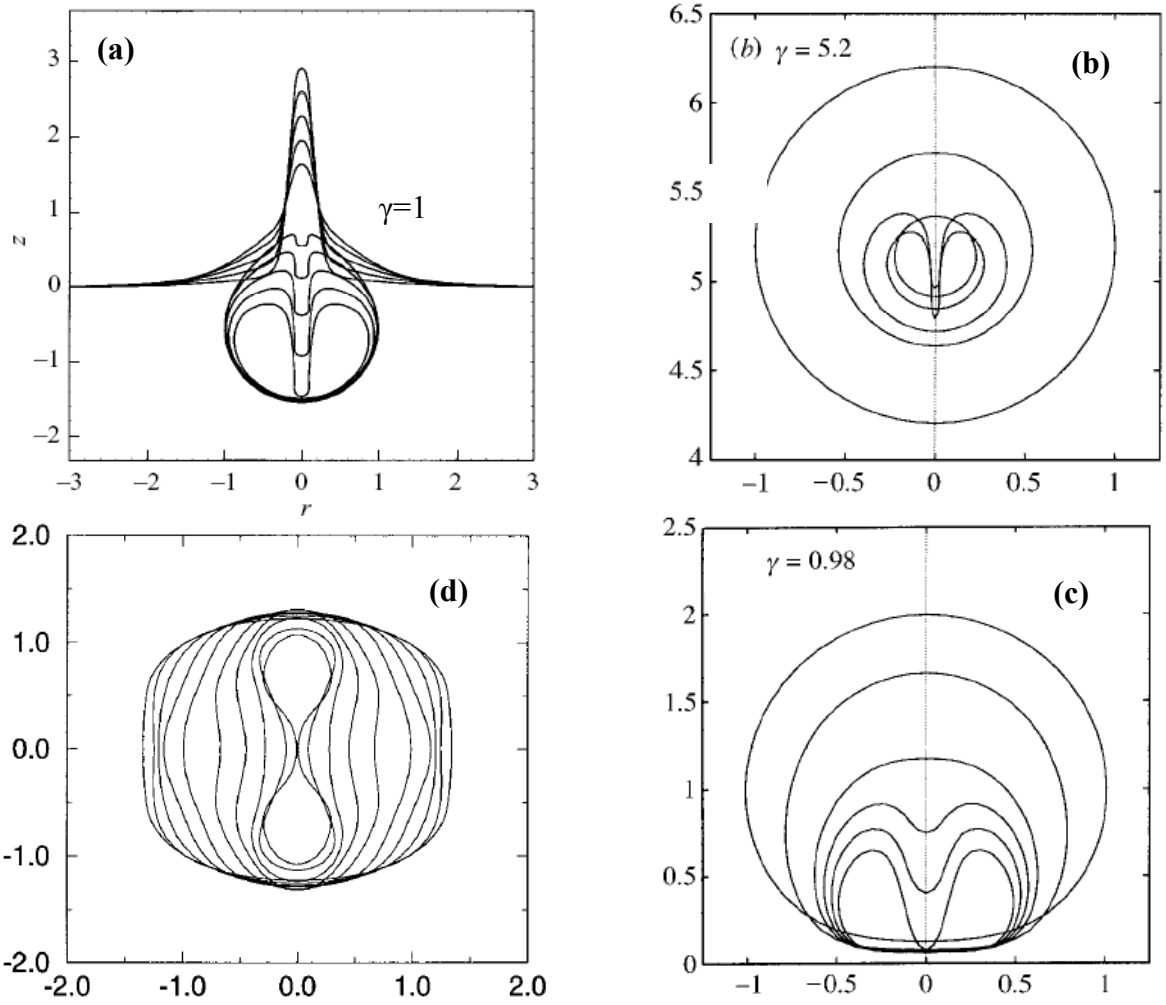

Figure 2: Bubble collapse (a) near a free surface, (b) far from a solid surface, (c) near a solid surface and (d) due to a radial disturbance on an initially oblate bubble. Figure 2a is reproduced from [12], Figures 2b,c from [59] and Figure 2d from [10].

Remarkable agreement with experimental observations has been achieved in boundary integral calculations of growth and detachment of a bubble from a submerged needle [63]. In a different context, finite element simulations combined with a quasi-elliptic mesh generation scheme provide a useful accuracy check on dynamic surface tension measurements from

supported bubbles [64]. A hybrid finite element approach was adopted that utilizes a combination of quasi-elliptic mesh generation [52] near the interface with algebraic mesh generation [49] far from it, in order to accommodate the severe accuracy requirements around the deformed bubble interface. In this case departure from sphericity or hydrodynamic effects may cause significant deterioration in the reliability of measurements. It should be noted, that in both the above flow situations bubble deformation is not nearly as severe as those observed in cavitation studies.

Volume oscillations of a bubble, as predicted by the Rayleigh-Plesset theory, are also known to become unstable and exhibit shape oscillations that reduce the validity of the assumption of spherosymmetry and that also may lead to bubble break-up depending on the intensity of the initial disturbance. That was first pointed out by *Plesset* [65] for inviscid oscillations and later on by *Prosperetti* [7] when weak viscous effects are included. In particular, a threshold amplitude is established beyond which different spherical harmonics grow, absorb energy from the primary volume oscillation and eventually dominate the dynamics while deforming the bubble shape. A Floquet type analysis reveals a phase diagram [66] regarding shape instability in the (R_0, P_A) space, that is dominated by the second Legendre mode, $P_2(\cos\theta)$. A prediction for the amplitude threshold for parametric instability to take place, valid for small amplitude oscillations and weak viscous effects, is provided in [8] as a function of, Re, the natural frequency of the shape mode, ω_n, and the frequency of volume oscillations Ω_0,

$$\varepsilon < \frac{2}{(4n-1)\omega_n}\left[2(2n+1)(n+2)\frac{1}{\mathrm{Re}^2}+(\Omega_0-2\omega_n)^2\right]^{1/2}. \qquad (41)$$

In the above formula surface tension is used in order to render time and velocity dimensionless, $\mathrm{Re}=\sqrt{\sigma R_0/(\rho\nu^2)}$, while Ω_0 denotes the dimensionless frequency of radial oscillations. As the amplitude of the initial pressure disturbance, P_A, increases the mode of instability switches to the Rayleigh-Taylor instability that is related to large positive radial accelerations and occurs near the minimum bubble radius. Another issue of great scientific and practical importance is that of coupling between shape and volume oscillations. When the bubble is forced away from resonance and the shape oscillations are either subharmonic, $2\omega_n=\omega_0$, or synchronous, $\omega_n=\omega_0$, with the radial oscillation, then shape oscillations are excited, on an $O(\varepsilon^{-1})$ time scale, with a frequency that is slaved to that of the radial motion [67]. When the forcing frequency is close to the natural frequency for volume oscillations then if the radial and shape modes are in exact two-to-one resonance the mixed motion is strictly periodic and is stable to axisymmetric perturbations [8]. In the presence, however, of a certain amount of detuning between them there is a range of forcing frequencies for which there is constant exchange of energy between the radial and the shape mode that may even lead to chaos [8]. These are interesting resonance phenomena that bear significance in establishing the appropriate range for spherosymmetric oscillations to exist in the context of many physical phenomena, most notably sonoluminescence, but also in understanding the ambient sound production in the upper ocean, *Longuet-Higgins* [68].

An effort to numerically investigate the above phenomena in the limit of potential theory was carried out in [9,10] in the presence of isotropic and non-isotropic pressure forcing, via the boundary integral and the spectral method. Indeed coupling effects were identified to exist for the appropriate frequency range, even when higher harmonics than the 2nd were examined in which case small amplitude theory is of limited value. Strong departures from the Rayleigh-Plesset theory were also identified at large disturbance amplitudes. In fact, mode interaction was seen to lead to break-up of an initially oblate spheroid bubble via formation of a toroidal bubble, Fig 2d, when the disturbance amplitude is increased beyond

the limit of weakly nonlinear theory. It should also be noted that the superior efficiency of the boundary integral over the spectral method in capturing large amplitude oscillations involving higher shape modes, was ascertained.

The appearance of shape instabilities as a result of isotropic pressure disturbances was examined in [41,42] via the boundary integral method in the context of inviscid and axisymmetric bubble-bubble interactions. When a small amplitude, $O(\varepsilon)$, step change in pressure, or a sinusoidal pressure disturbance with an off-resonance frequency ω_f, is applied, subharmonic resonance is almost invariably observed between radial oscillations and the shape mode for which the condition $2\omega_n = \omega_0$ or $2\omega_n = \omega_f$ holds, as predicted in [67]. The bubble shape reflects the excitation of the appropriate mode, e.g. 9^{th} and 10^{th} modes for the left bubble in Fig 3, on an $O(\varepsilon^{-1})$ time scale. When the disturbance amplitude is further increased the two bubbles are seen to accelerate as a result of the secondary Bjerknes forces between them, as an $O(\varepsilon^2)$ effect. The forces exerted on the two bubbles are equal in magnitude but opposite in direction and consequently the smaller bubble experiences a larger acceleration. As the acceleration of either one of the bubbles increases beyond a certain threshold value, identified as a Bond number relating acceleration to surface tension, a Rayleigh-Taylor type instability arises and the bubble shape exhibits strong anisotropy which in extreme cases takes the form of spherical-cap shapes. For instance, in Fig 3 the right bubble is smaller and consequently accelerates faster than the left one and acquires a spherical-cap shape. Such shapes are characterized by an almost spherical front, whereas the side facing away from the direction of acceleration exhibits areas of small curvature and shape oscillations. There is also indication of bubble break-up and formation of satellite bubbles. This is an interesting result that might bear some significance in the rising bubble problem where shape oscillations are associated with path instabilities. Of course it remains to be seen how weak viscous effects will affect this behaviour.

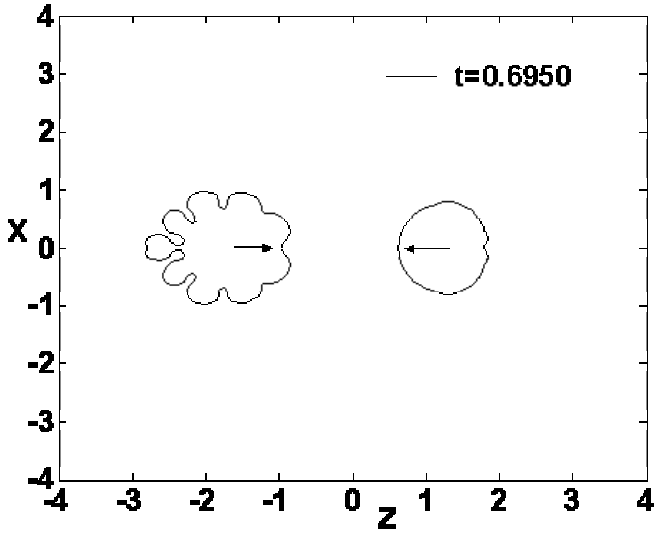

Figure 3: Bubble-bubble interaction after a step change in the atmospheric pressure; $P_\infty=P_{St}(1+0.3)$, $R_{02}/R_{01}=0.8$, $\gamma=D/R_{01}=4$, $R_{01}=1$ mm (reproduced from [42]).

The effect of weak viscous dissipation on bubble collapse and break-up was recently examined in an investigation of the dynamics of elongated bubbles under negligible or large internal overpressures [17,18]; intensity of elongation is measured via the ratio, S, between the bubble equilibrium radius and the long axis of the ellipsoid produced by elongation. Thus, a threshold initial elongation was discovered below which the bubble performs oscillations with energy being exchanged between the zeroth and the 2^{nd} Legendre modes and the bubble

eventually relaxing to its spherosymmetric equilibrium state. For more intense elongation two fast jets are formed that propagate in opposite directions along the axis of symmetry and meet at the equatorial plane forming a microbubble surrounded by a larger bubble of toroidal shape, Figs 4a,b,c. Evidence was also presented, [17], that during the final stages of collapse, surface tension and convection balance each other and produce a universal interdependence between the time and space scales [69]. Viscosity decelerates the speed of the jet and produces a critical Re below which the jets do not touch [17].

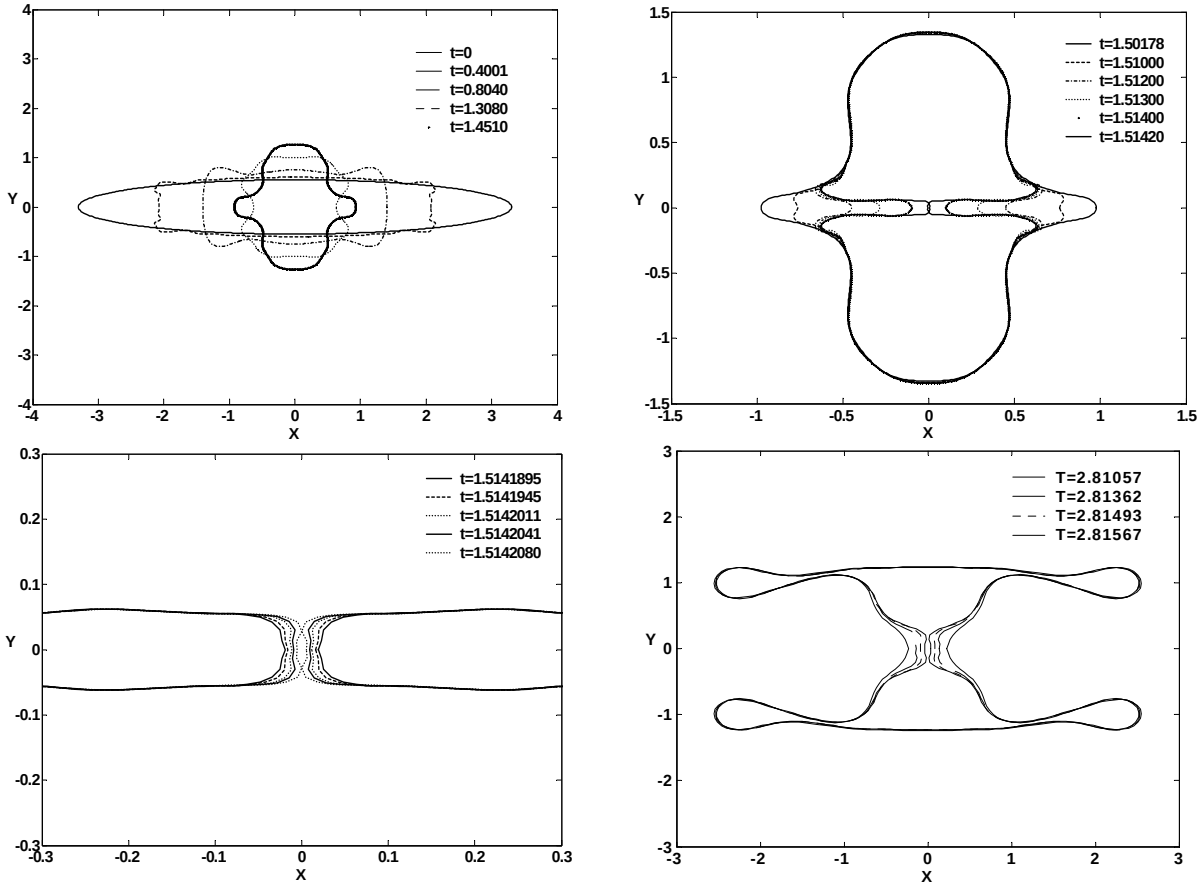

Figure 4: Inviscid simulation of an elongated bubble at atmospheric pressure (a) in the beginning of the motion, (b) during jet formation and (c) during collapse (R_0~5μm, S=0.6, reproduced from [17]); (d) with internal overpressure of 40 atm and severe elongation (S~0.34, reproduced from [18])

The case with large internal overpressure was also investigated, [18], since it is relevant to sonoluminescence experiments with laser bubbles [70]. In this flow arrangement aspherical bubble collapse is observed, yet the bubbles luminesce at the bubble site of jet impact, an effect that was conjectured to be due to the formation of tiny microbubbles. Additional evidence in support of this supposition is provided by the simulations carried out in [18], when weak viscous effects are included and large internal overpressures are considered in conjunction with very large initial elongations. Inviscid simulations reveal a collapse mode where the incoming jets are deflected and hit the bubble walls. Including weak viscous dissipation favors a collapse mode similar to the case of zero internal overpressure, in the sense that the regions near the two poles accelerate and eventually meet at the equatorial plane, before they turn and hit the bubble walls, to form a tiny microbubble surrounded by a larger toroidal bubble, Fig 4d. Currently, these simulations are extended to account for the effect of elasticity on the bubbles interface, as required for the investigation of the dynamic

behaviour of contrast agents. An interesting parallelism between parametric instability of bubbles and buckling of spherical shells is under investigation in this context, [71].

The effect of secondary Bjerknes forces on the translational motion of the bubbles was also examined in [41,42] and the classical Bjerknes theory, wherein bubbles attract or repel each other depending on whether they oscillate in or out of phase, was verified. In addition, conditions for the formation of stable bubble pairs were sought after, in the light of the theory by *Doinikov & Zavtrak* [72]. It the latter study, it was shown, for bubbles insonated by a forcing frequency above their resonance frequencies, that as their distance decreases a point is reached beyond which their mutual force changes sign becoming repulsive until they get far enough for attraction to prevail again and the cycle to be repeated. Boundary integral simulations performed in [41,42] verified that this is indeed the case for small amplitude oscillations. This effect cannot be predicted by classical Bjerknes theory since it is valid when the distance between the bubbles is infinitely large. *Doinikov & Zavtrak* explained it by accounting for the multiple scattering interaction between the bubbles in the context of linear theory, in terms of the variation of the two natural frequencies as the distance between the bubbles decreases. This is indeed the case when the two bubbles are driven above resonance. However, this argument cannot explain the change in the sign of the force at small distances when the forcing frequency falls in the range of the two natural frequencies since then, by linear theory [41], as their distance decreases the eigenfrequency of the larger bubble decreases while that of the smaller increases and the forcing frequency always remains within their interval. More recently, a generalized theory was presented, [73], utilizing the 'transition frequencies', namely those for which there is a phase difference of $\pi/2$ between a bubble's pulsations and the external field. Thus, it was seen that a third transition frequency exists for each bubble, apart from the two natural frequencies for radial oscillations of the two individual bubbles, that collapses to one of the natural frequencies as the distance between them tends to infinity. In a subsequent article [74] the same investigator conducted a numerical study on the axisymmetric interaction of two bubbles in a viscous liquid, considering compressibility effects in both phases. A hybrid advection scheme was employed in conjunction with a multi-step integration technique and a front tracking approach for the location of the interface. The simulations, conducted for the case of small disturbance amplitude, show evidence that there is an additional transition frequency. Nevertheless, further research is required in order to establish the validity and practical significance of its effect.

IV.2 Bubble interaction with an external flow

Research in this area investigates bubble interaction with an external flow, e.g. shear or elongational among others, and this includes the rising bubble problem where it is the bubble itself that undergoes rectilinear motion, at least for small radii before path instabilities arise [28]. In this class of problems bubble oscillations are not of primary interest. Rather, the effect of viscous dissipation on the wake structure is of interest, both as a fundamental problem that distinguishes interfaces where slip is allowed from solid surfaces, but also as a means to obtain useful predictions for the drag and lift coefficients that can be used as input in larger models for bubbly flow. As an additional problem of fundamental importance the appearance of path instabilities in rising bubbles should be singled out, since it is intimately associated with interesting dynamic phenomena such as shape oscillations and wake stability. As a result of the nature of the problem, full Navier-Stokes solvers have been developed for its investigation, typically coupled with elliptic mesh generation in order to capture possible deformations of the bubble surface. A first step in this direction was taken by *Ryskin & Leal* [22,23], who developed a finite difference code coupled with a boundary fitted mesh generation scheme to study the buoyancy driven motion of a bubble in a quiescent liquid. In

this fashion they were able to calculate steady axisymmetric shapes of bubbles for a wide range of Re and We numbers (Re<200, We<20). Some of the experimentally observed shapes, in the range of small and intermediate Re, were reproduced but non-existence of steady axisymmetric shapes leading to spherical-cap shapes could not be established. It should be pointed out that the shapes obtained as Re increased where quite similar with the steady shapes obtained by *Miksis et al.* [21] with the boundary integral method including weak viscous effects. A very important finding of the full Navier-Stokes solution, however, that cannot be captured by weak viscous analysis is the discovery of flow separation behind the bubble for the intermediate range of Re and large enough $We=2\rho U^2R_0/\sigma$ numbers, Fig 5.

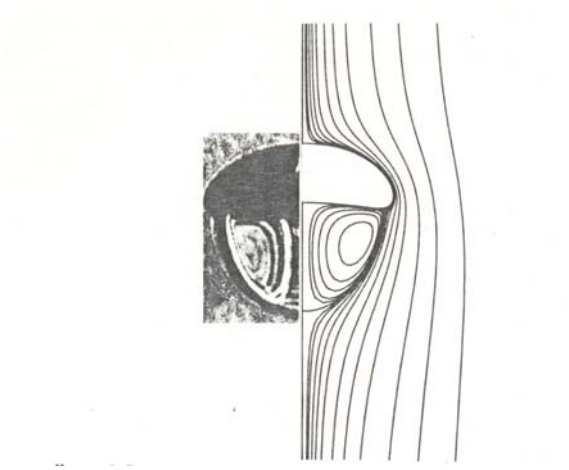

Figure 5: Comparison of experimental measurements (Hnat & Buckmaster, Phys. Fluids 19, 1976) and numerical predictions for the shape and the wake behind a rising bubble (Re~20, We~15, reproduced from [23]).

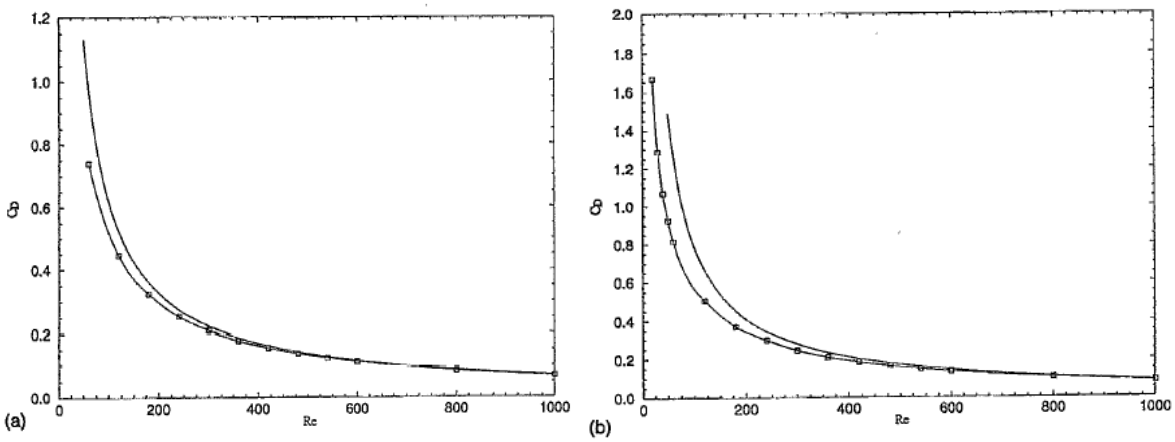

Figure 6: Drag coefficient C_D as a function of Re, (a) χ=1.5 and (b) χ=1.75; ——— Moore's theory, —•— numerical results (reproduced from [47]).

It was already known from *Moore's* early work, [20], that the boundary layer around a spherical bubble does not separate. Assuming that no separation takes place, the same investigator proceeded in a later study and obtained an expression for the drag coefficient around spheroid bubbles

$$C_D=\frac{48}{Re}G(\chi)\left[1+\frac{H(\chi)}{Re^{1/2}}+o\left(\frac{1}{Re^{1/2}}\right)\right],\quad Re=\frac{2R_0U\rho}{\mu},\quad C_D=\frac{Drag}{\frac{1}{2}\rho U^2\pi R_0^2},\quad \chi=\frac{c}{a} \qquad (42)$$

with χ denoting the ratio of the cross stream to the parallel axis of the spheroid, [75]. A question was then raised regarding the lower bound on Re for the validity of this assumption and how this bound changed as the bubble shape became more and more oblate. This issue was settled by *Dandy & Leal* [48], by employing the numerical methodology developed by *Ryskin & Leal*, wherein it was shown that a threshold value of Re exists below which standing eddies are formed behind the bubble, in marked disagreement with what is known from solid boundaries. In fact, formation of eddies is restricted within a specific interval of Re and is quite distinct from boundary layer separation. Recent developments of elliptic mesh generation techniques [45,46] allowed simulations to proceed to higher Re. In particular, *Magnaudet et al*. [25] and *Blanco & Magnaudet* [47] utilized a finite volume approach with an improved elliptic mesh generation scheme to solve viscous flow around, a spherical bubble recovering *Moore's* theory for Re>50, and around an ellipsoidal bubble of fixed shape for Re up to 1000, respectively. In the latter study it was shown that as the oblateness of the bubble increases the threshold in Re beyond which *Moore's* theory is correct increases as well, Fig 6. The evolution of the wake structure was recovered for the range of Re numbers over which it exists, and the growth and eventual disappearance of its size over the same region was clearly illustrated, Fig 7. Interestingly enough it was discovered that even though the shape of the bubble had a significant effect on the drag coefficient the standing eddy did not have any noticeable influence.

Blanco & Magnaudet [47] used a dynamic code and investigated the possibility for unsteadiness in their results also, which was not possible. A similar time dependent axisymmetric study, based on a boundary fitted mesh, was conducted by *Takagi et al*. [24]. The numerical simulations of the latter investigators suggest the onset of axisymmetric shape oscillations leading towards three dimensional path instabilities. Recent experimental observations [28] obtain the critical values of Reynolds for zig-zag or spiral paths to arise and provide the bubble shapes and terminal velocities as a function of the radius of rising bubbles. In fact, the latter look quite similar with graphs obtained in [21] with the boundary integral method including *Moore's* prediction for the viscous drag coefficient. It should also be noted that zig-zag paths seem to arise as an instability of rising bubbles with almost spherical shape [28] in which case standing eddies do not exist. In fact as the bubble size increases, R_0>4 mm, experimental observations [27] indicate that vortex shedding frequency is locked to the frequency of shape oscillations. In view of the above findings it is the author's opinion that an axisymmetric time dependent solution via the boundary integral method, one that also accounts for weak viscous effects, will provide the proper steady bubble shapes, but also spherical-cap shapes exhibiting shape oscillations in the upstream region. Steady shapes can be used for carrying out a stability analysis that allows for three-dimensional fully viscous perturbations. In this framework the bifurcation points that lead to path instabilities may be provided. Owing to the distorted shape as Re increases the quasi-elliptic mesh generation approach will be favorable for providing the proper resolution of the boundary layer and wake regions around the bubble that will emerge as part of the bifurcating solutions. On the other hand, the onset of spherical-cap shapes, and the shape oscillations associated with them can be used as a means to capture the critical value of Reynolds for path instabilities of large bubbles. In all likelihood, in this case the behaviour of the wake is not needed for capturing the onset of path instability. Rather, this is a result of neighboring shape mode interaction that triggers the erratic translational motion of the bubble in the presence of temporal and spatial phase drift. This mechanism can be predicted in the context of potential theory as was first implied by *Saffman* [31] and rigorously shown by *Benjamin & Ellis* [32]. More recently, Feng & Leal [76] extended these ideas to include the effect of resonance between the interacting shape modes and the forcing frequency, while *Doinikov* [77] accounted for the combined effect that shape oscillations and translation may have on volume pulsations and

discussed its implications on ambient oceanic noise, [68]. A three-dimensional boundary integral type simulation would be very useful in examining these effects in more detail.

In a different context, three-dimensional dynamic simulations of single bubble interaction with external flows using an elliptic mesh generation scheme have been carried out [26], in order to obtain accurate predictions of the drag and lift coefficients over a wide parameter range. Agreement with previous asymptotic formulas is validated and, more importantly, improvements of previously available empirical correlations are derived. Such efforts constitute a very useful first step in producing the necessary interaction forces for numerical simulation of bubbly flows.

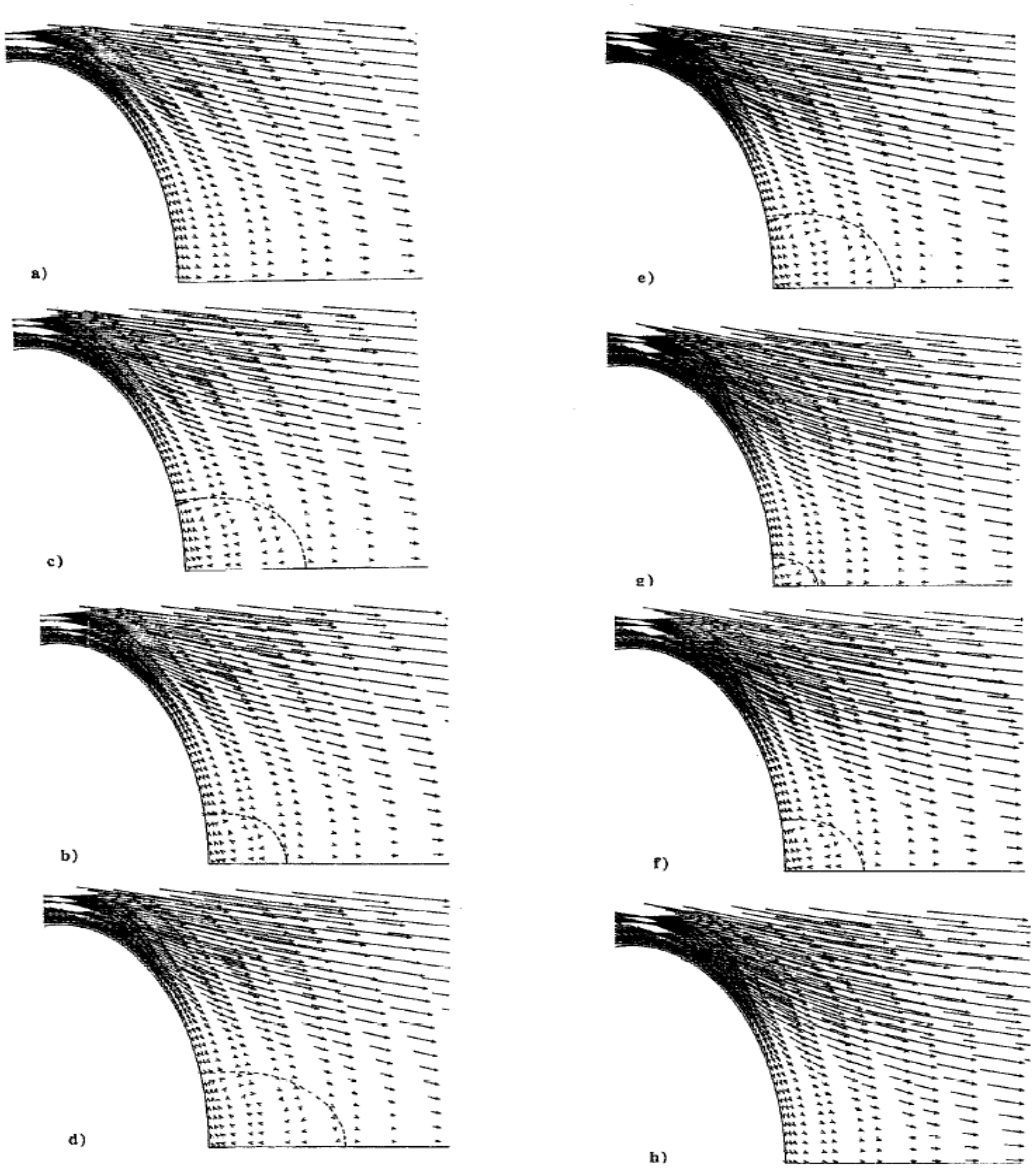

Figure 7: The flow at the rear of an ellipsoidal bubble of aspect ratio χ=1.75 (dashed lines delimit the separation region) (a) Re=60; (b) Re=75; (c) Re=100; (d) Re=150; (e) Re=200; (f) Re=300; (g) Re=350; (h) Re=400 (reproduced from [47]).

The method of Galerkin finite elements coupled with the fixed spine method [49] was recently applied, [50], in order to capture the physics of bubble deformation inside a viscoelastic filament that undergoes stretching with a constant pulling velocity. Such a flow arrangement is believed to arise in the process of fibrillation of block copolymer adhesives.

The effect of material viscoelastic properties on bubble dynamics is presented and the role of bubble growth and deformation on the bulk material properties is discussed.

IV.3 Numerical Experiments with Rising Bubbles

It should be pointed out that direct numerical simulations of bubble dynamics can be performed with the numerical techniques described in sections III.1 and III.2. However, we reserve the term numerical experiments for the interface tracking schemes presented in III.3 since they can capture more complicated topological changes such as the post break-up or post coalescence flow structures. Simulations on bubbly flows and bubble merging have been carried out in the past, see for example [33, 78]. Nevertheless, most of the available numerical data have been obtained from simulations of the rising bubble problem which has become a test case for direct numerical simulations with deforming interfaces, due to the wealth of theoretical, experimental and numerical studies with more conventional numerical methodologies that are available for direct comparison.

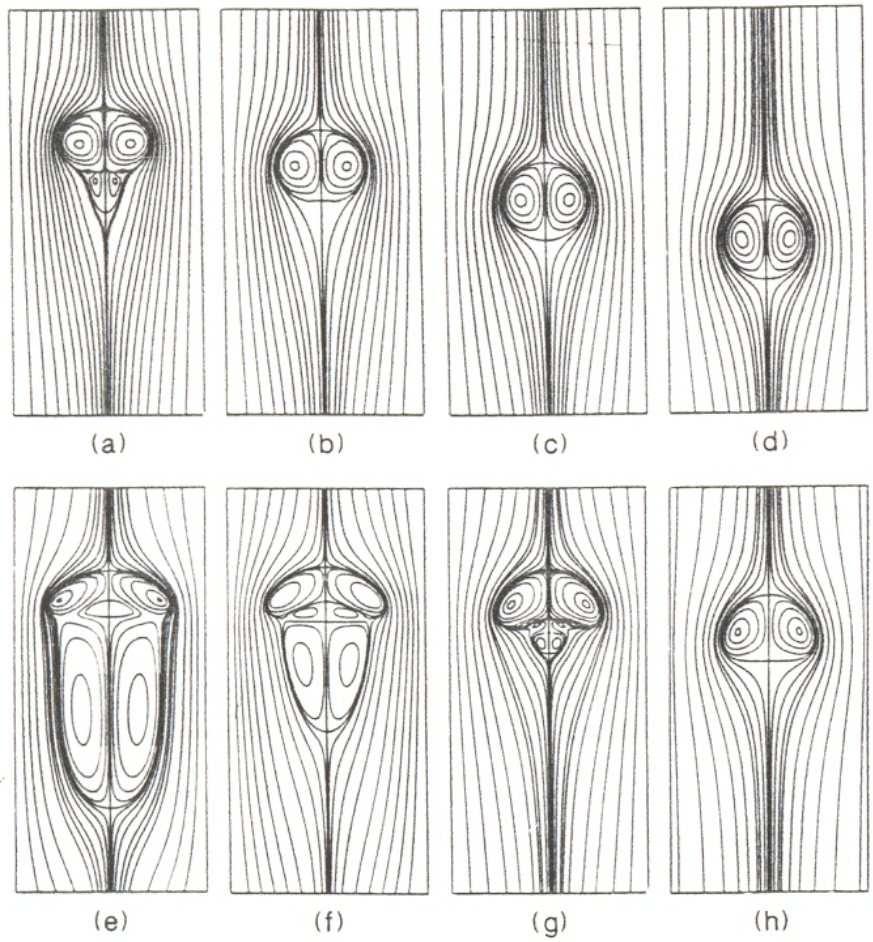

Figure 8: Stream lines for a two-dimensional steadily rising bubble under various Eo and M numbers, ρ/ρ_b=40 and. Top row, Eo=1; (a) μ/μ_b=88 and M=10^{-7}; (b) μ/μ_b=156 and M=10^{-6}; (c) μ/μ_b=277 and M=10^{-5}; (d) μ/μ_b=493 and M=10^{-4}. Bottom row, Eo=10; (a) μ/μ_b=88 and M=10^{-4}; (b) μ/μ_b=156 and M=10^{-3}; (c) μ/μ_b=277 and M=10^{-2}; (d) μ/μ_b=493 and M=10^{-1} (reproduced from [33]).

Early studies in this field concentrated on simulations of two-dimensional bubbles and parameter ranges, e.g. viscosity μ/μ_b and density ρ/ρ_b ratios, Morton and Eotvos numbers, that were somewhat restrictive, [33,34,35,57,79]. As was mentioned before, in the context of

the rising bubble problem gravitational forces provide the characteristic velocity in which case,

$$\mathrm{Re}=\frac{\rho\sqrt{gR_0}R_0}{\mu},\quad \mathrm{We}=\frac{\rho gR_0^2}{\sigma}=\frac{\rho g\left(d_0/2\right)^2}{\sigma}=\frac{\mathrm{Eo}}{4}. \tag{43}$$

Quite often the Morton is used instead of Re

$$\mathrm{M}=\frac{\mathrm{Eo}^3}{\mathrm{Re}^4}=\frac{\left(\rho g\right)^3 d_0^6}{\sigma^3}\frac{\mu^4}{\rho^4 g^2 d_0^6}=\frac{g\mu^4}{\rho\sigma^3} \tag{44}$$

that depends solely upon the properties of the surrounding medium. *Bhaga & Weber* [80] presented a graphical correlation that mapped the (Re, Eo) space into different regimes according to the dynamic behaviour of bubbles rising in different quiescent liquids. This semi-empirical map provides a means for comparing numerical simulations against well-established knowledge in this field.

Previous numerical simulations by the boundary integral method [21] and by boundary fitted coordinates [22,23,24,81] have recovered spherical and oblate spheroid or ellipsoidal steady shapes. In the latter two cases, [24,81], there is evidence from axisymmetric dynamic simulations, that shape oscillations arise and trigger path instabilities. Surface tracking techniques [33,34,35,57] originally tried to solve two dimensional models in order to recover the wake structure revealed by boundary fitted mesh generation techniques, most notably the results of *Ryskin & Leal* [22,23]. This had encouraging results [33], Fig 8, hence the method has been extensively applied in axisymmetric and three-dimensional geometries [33, 78] albeit for a relative narrow parameter range, in order to investigate its qualitative behaviour and its convergence upon mesh refinement. More recently, a combination of the level-set and the volume of fluid methods on an adaptive grid has been applied on three-dimensional simulations of rising bubbles [36] over a considerable range of the *Bhaga & Weber* diagram with impressive findings. In particular, the dynamic evolution of an initially spherical bubble that rises in a quiescent fluid into an 'oblate spheroid', 'oblate ellipsoidal disk-like and wobbling' and 'oblate ellipsoidal cap' was captured for the range of Re and Eo predicted in [80]. In the low M and intermediate Eo region zig-zag and spiral paths are obtained for bubble shapes that appear to be close to the spherical and ellipsoidal shapes observed in [28], Fig. 9. Finally, depending on the initial conditions an initially spherical or 'oblate ellipsoidal cap' bubble was seen to evolve into a toroidal or a spherical-cap bubble, respectively, in the low M and large Eo regime, Fig. 10. The appearance of such shapes has been anticipated by previous experimental and numerical investigations as well as their dependence on initial conditions. In the case of spherical-caps the simulations clearly indicate the formation of satellite bubbles behind the bubble in accordance with experimental observations. Based on the above findings there is evidence that this class of numerical methods is reaching its maturity and can provide data that we would like to get from 'numerical experiments'.

The above simulations suffer from the drawback that they all ignore compressibility of the material inside the bubble. Of course, this is not an important issue when the problem of a rising bubble is studied, where bubble oscillations are not expected to play such a central role, at least when Re is not very large for shape oscillations to occur. Nevertheless, there have been developments in this direction both in the context of the surface tracking techniques [55] but also in the emerging field of Lattice-Bolzmann simulations [79] where compressibility is inherently included in the model. Such efforts have not yet reached the point where they can be directly compared against existing experimental or numerical studies. However, they are considered as promising alternatives owing to their fundamental nature.

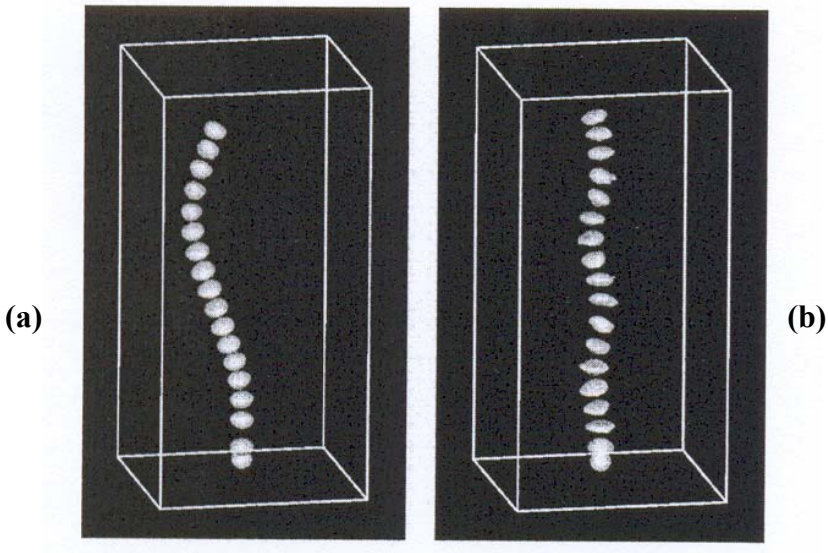

Figure 9: Examples of zig-zag and spiral bubble motion at low Morton numbers, Mo=1.9x10^{-10}; (a) Re=700, Eo=1.9 and (b) Re=1000 and Eo=7.5 (reproduced from [36]).

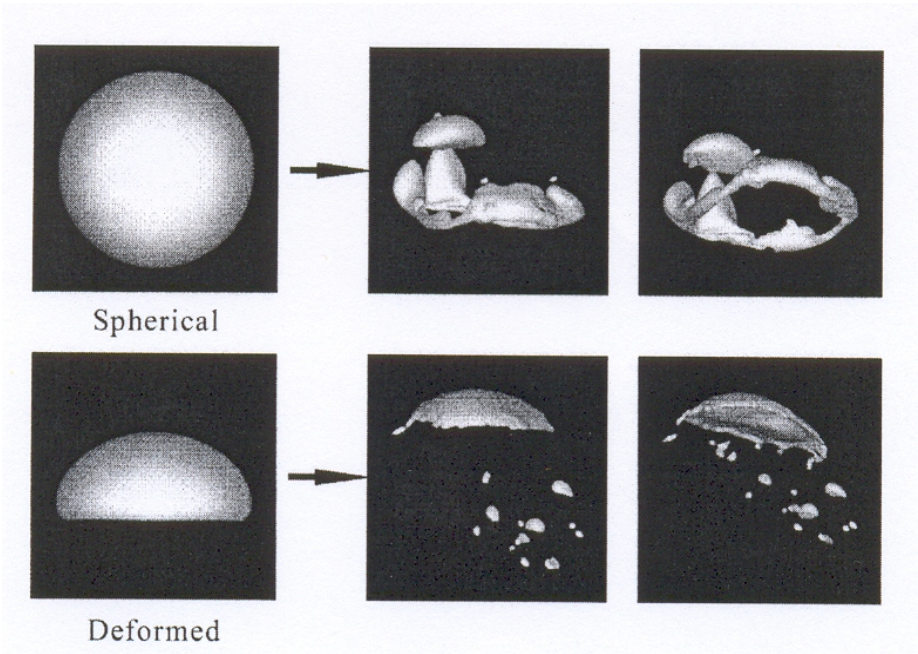

Figure 10: Numerical results for eo=182 and m=9.9x10^{-6} depending on the initial conditions (reproduced from [36]).

V. CONCLUSIONS

As an overall remark on the contribution of numerical techniques to our knowledge regarding bubble dynamics, it should be stressed that they have significantly enhanced our understanding of fundamental issues such as interfacial instabilities, bubble collapse and break-up and the wake structure behind deformed free surfaces. In addition, carefully designed numerical experiments have recently emerged as an alternative to experiments for flow situations that are not easily controlled in the laboratory, either by incorporating numerically obtained correlations of the drag and lift coefficients in models of bubbly flows or by utilizing modern surface tracking and reconstruction schemes.

In particular, the boundary integral method seems to be more efficient when isotropic disturbances are applied or when specific details are demanded of severely deformed interfaces. Thus, boundary elements have been used to capture the nature of bubble collapse near a solid or a free boundary and to illustrate the importance of jet impact on the damaging effect of a cavitating bubble. The same methodology has been applied for the evaluation of the importance of available interfacial instability mechanisms, i.e. parametric and Rayleigh-Taylor instabilities. The details of break-up of a bubble subjected to an acoustic disturbance or an initial elongation have also been monitored in the same fashion and the formation of satellite microbubbles has been pointed out along with their significance on sonoluminescence. The same approach has afforded the investigation of universalities in the final stages of bubble break-up as an extension of existing theories for drop pinch-off. Inclusion of weak viscous effects that account for the normal viscous stress and viscous pressure correction has significantly extended the range of validity of the boundary integral method for problems involving free surfaces.

When the wake structure is needed and its impact has to be accounted for on the path of a bubble undergoing translational motion or on the drag and lift coefficients of a bubble, then resorting to a full Navier-Stokes solver is necessary. This guarantees applicability over a wide range of Reynolds provided the shape deformation of a moving bubble is captured at the same time. This has led to the development of a number of elliptic mesh generation schemes that provide boundary fitted coordinates that follow the shape of the bubble and preserve orthogonality properties. In this fashion the nature of standing eddy formation behind deformed interfaces has been understood and the range of Reynolds over which it occurs has been accurately predicted. Three-dimensional simulations have been performed for bubbles interacting with different types of external flows with important results from the fundamental perspective but also from a more practical point of view, regarding the production of semi-empirical correlations for drag and lift coefficients that can be utilized in bubbly flow models. Application of quasi-elliptic mesh generation schemes that satisfy conditions of smoothness and density of the coordinate lines seems to be a promising adjustment that will allow more accurate description of highly deformed interfaces.

Until recently use of boundary fitted coordinate systems seemed to be the only way to perform direct numerical simulations of bubble dynamics. The appearance of surface tracking techniques, e.g. front-tracking, volume-of-fluid and level-set methods, has extended the range of applicability of numerical simulations by affording simulation of severe topological changes such as coalescence or the formation of satellite bubbles. As a benchmark problem that of the bubble that rises in an otherwise quiescent fluid has been employed in order to test the validity of these methods, with very encouraging results thus far. Situations with spherical bubbles, oblate ellipsoidal, wobbling, toroidal or spherical-cap shape bubbles have been successfully resolved. At the current stage of their development these methods are now required to systematically provide useful details of flow situations that cannot be otherwise predicted and for the appropriate material properties.

In the author's opinion numerical simulations have reached a stage where we can get specific answers to specific and realistic problems. More importantly, besides existing areas of research there are new exciting fields that require proper modeling of bubble dynamics, as, for instance, the application of contrast agent imaging in modern echocardiography. What is now required is the ability to employ different techniques depending on the type of answer we need. For example, in the rising bubble problem we need to be able to numerically reproduce the exact regimes corresponding to the appearance of a certain type of bubble shape. This has been done experimentally [27,28,80] and there is every indication that it will soon be done numerically [36]. Extensive use of parallel computing is expected to accelerate this process. However, we also need to know the precise mechanism behind each transition.

In particular, it still has to be unequivocally determined (a) what is the parameter range for which the wake imposes its dynamics on the bubble and (b) what is the parameter range for which the opposite happens. There are indications that for small bubbles the wake determines the dynamics whereas for larger bubble shape oscillations set in and they trigger wake instabilities. This is something that can be determined in the light of a theoretical approach that will employ simplified models specifically designed to investigate a specific mechanism. Nevertheless, this has been made possible only because there has been a built up of knowledge on this problem, based on extensive numerical and experimental studies that point out the appropriate parameter range and the appropriate natural forces for the theory to focus on. Consequently, we need to be able to exploit the synergies that arise from modern computational and theoretical advances in the field of bubble dynamics in order to obtain answers to physical problems of fundamental importance but also to create software that can be useful in modern technical applications.

REFERENCES

1. Strutt, J.W. (Lord Rayleigh) 1917, *Philos. Mag.* **34**, 94.
2. Leighton, T.G. 1994, *The acoustic bubble,* Academic Press.
3. Ohl, C. D., Kurz, T., Geisler, R., Lindau, O. & Lauterborn, W. 1999, 'Bubble dynamics, shock waves and sonoluminescence,' *Phil. Trans. R. Soc. Lond. A*, **357**, 269-294.
4. Suslick, K. S. 1990, 'Sonochemistry,' *Science*, **247**, 1439-1445.
5. Goldberg, B.B., Raichlen J.S. & Forsberg F. 2001, *Ultrasound Contrast Agents: Basic Principles and Clinical Applications*. Dunitz Martin Ltd, London, UK.
6. Tachibana, Li.T. & Kuroki, M. 2003, 'Gene transfer with echo-enhanced contrast agents: Comparison between Albunex, Optison and Levovist in mice-initial results,' *Radiology* **229**, 423-428.
7. Prosperetti, A. 1977, 'Viscous effects on perturbed spherical flows,' *Quarterly of Applied Mathematics*, **35**, 339-352.
8. Feng, Z.C. & Leal, L.G. 1994, 'Nonlinear bubble dynamics,' *Annu. Rev. Fluid Mech.* **29**, 201-243.
9. McDougald N.K. & Leal G.G. 1999, 'Numerical study of the oscillations of a non spherical bubble in an inviscid incompressible liquid. Part I: free oscillations from non-equilibrium initial conditions,' *Int. J. Multiphase Flow* **25**, 887-919.
10. McDougald N.K. & Leal G.G. 1999, 'Numerical study of the oscillations of a non spherical bubble in an inviscid incompressible liquid. Part II: the response to an impulsive decrease in pressure,' *Int. J. Multiphase Flow* **25**, 921-941.
11. Blake, J.R. & Gibson, D.C. 1987 'Growth and collapse of a vapour cavity near a free surface,' *J. Fluid Mech.* **111**, 123-140.
12. Blake, J.R., Hooton M.C., Robinson, P.B. & Tong, R.P 1997, 'Collapsing cavities, toroidal bubbles and jet impact,' *Phil. Trans. R. Soc. Lond. A.* **355**, 537-550.
13. Wu, C. C. & Roberts, P. H. 1994, 'A model for sonoluminescence,' *Proc. R. Soc. Lond. A* **445**, 323-349.
14. Plesset, M.S. & Prosperetti, A. 1977, 'Bubble dynamics and cavitation,' *Annu. Rev. Fluid Mech.* **9**, 145-185.
15. Boulton-Stone, J.M. & Blake, J.R. 1993, 'Gas bubbles bursting at a free surface,' *J. Fluid Mech.* **254**, 437-466.
16. Lundgren T.S. & Mansour, N.N. 1988, 'Oscillations of drops in zero gravity with weak viscous effects,' *J. Fluid Mech.* **194**, 479-510.
17. Tsiglifis K. & Pelekasis, N. 2004, 'Weak viscous oscillation and collapse of elongated bubbles under small initial overpressure', to appear in the *Physics of Fluids.*
18. Tsiglifis K. & Pelekasis, N. 2005 'Weak viscous oscillation and collapse of elongated LASER bubbles,' to be submitted to the *Physics of Fluids.*
19. Magnaudet, J. & Eames, I. 2000, 'The motion of high-Reynolds-number bubbles in inhomogeneous flows,' *Annu. Rev. Fluid Mech.* **32**, 659-708.
20. Moore, D.W. 1963, 'The boundary layer on a spherical gas bubble,' *J. Fluid Mech.* **16**,161-176.
21. Miksis, M.J., Vanden-Broeck J.M. & Keller, J. 1982, 'Rising bubbles,' *J. Fluid Mech.*, **123**, 31-41.
22. Ryskin, G & Leal, G.L. 1984, 'Numerical solution of free boundary problems in fluid mechanics. Part 1: The finite-difference technique,' *J. Fluid Mech.* **148**, 1-17.
23. Ryskin, G & Leal, G.L. 1984, 'Numerical solution of free boundary problems in fluid mechanics. Part 2: Buoyancy-driven motion of a gas bubble through a quiescent liquid,' *J. Fluid Mech.* **148**, 19-35.

24. Takagi, S., Matsumoto, Y & Hung. H.X. 1997, 'Numerical analysis of a single rising bubble using boundary-fitted coordinate system,' *JSME Int. J Series B-Fluids and Thermal Eng.* **40**(1), 42-50.
25. Magnaudet, J., Rivero, M. & Fabre, J. 1995, 'Accelerated flows past a rigid sphere or a spherical bubble. Part 1. Steady straining flow,' *J. Fluid Mech*. **284**, 97-135.
26. Legendre, D. & Magnaudet, J. 1998, 'The lift force on a spherical bubble in a viscous linear shear flow,' *J. Fluid Mech*. **368**, 81-126.
27. Lunde, K. & Perkins, R. 1998, 'Shape oscillations of rising bubbles,' *Appl. Sci. Res*. **58**, 387-408.
28. Wu, M. & Gharib, M. 2002, 'Experimental studies on the shape and path of small air bubbles rising in clean water,' *Physics of Fluids* **14**(7), L49-L52.
29. Saffman, P.G. 1956, 'On the rise of small air bubbles in water,' **1**, 249-275.
30. Eller, A.I. & Crum, L.A. 1970, 'Instability of the motion of a pulsating bubble in a sound field,' *J. Acoust. Soc. Am*. **47**, 762-767.
31. Saffman, P.G. 1967, 'The self propulsion of a deformable body in a perfect fluid,' *J. Fluid Mech.* **28**, 385-389.
32. Benjamin, T.B. & Ellis, A.T. 1990, 'Self-propulsion of axisymmetrically vibrating bubbles,' *J. Fluid Mech*. **212**, 65-80.
33. Unverdi, S.O. & Tryggvason, G. 1992, 'A front-tracking method for viscous incompressible multi-grid flows,' *J. Comp. Phys*. **100**, 25-37.
34. Puckett, E.G., Almgren A.S., Bell, J.B., Marcus, D.L. & Rider, W.J. 1997, 'A high order projection method for tracking fluid interfaces in variable density incompressible flows,' *J. Comp. Phys*. **130**, 269-282.
35. Sussman, M. & Puckett, E.G. 2000, 'A coupled level set and volume-of-fluid method for computing 3d and axisymmetric incompressible two-phase flows,' *J. Comp. Phys*. **162**, 301-337.
36. Ohta, M., Haranaka, S., Yoshida, Y. & Sussman, M. 2004, 'Three-dimensional numerical simulations of the motion of a gas bubble rising in viscous liquids,' *J. Chem. Eng. Japan* **37**(8), 968-975.
37. Batchelor, G.K., 1967, *An introduction to fluid dynamics*, Cambridge University Press.
38. Lundgren, T. S. & Mansour, N. N. 1988, 'Oscillations of drops in zero gravity with weak viscous effects,' *J. Fluid Mech*. **194**, 479-510.
39. Pelekasis, N. A., Tsamopoulos, J. A. & Manolis, G. D. 1992, 'A hybrid finite- boundary element method for inviscid flows with free surface,' *J. Comp. Phys*. **101**(2), 231-251.
40. Brebbia, C.A. 1978, *The boundary element method for engineers*, Halsted Press.
41. Pelekasis, N. A. & Tsamopoulos, J. A. 1993, 'Bjerknes forces between two bubbles. Part 1: Response to a step change in pressure,' *J. Fluid Mech*. **254**, 467-499.
42. Pelekasis, N. A. & Tsamopoulos, J. A. 1993, 'Bjerknes forces between two bubbles. Part 2: Response to an oscillatory pressure field,' *J. Fluid Mech*. **254**, 501-527.
43. Pope, S.B. 1978, 'The calculation of turbulent recirculating flows in general orthogonal coordinates,' *J. Comput. Phys*. **26**, 197-212.
44. Ascoli, E.P., Dandy, D.S. & Leal, G.L. 1987, 'On distortion functions for the strong constraint method of numerically generating orthogonal coordinate grids,' *J. Comput. Phys*. **72**, 513-519.
45. Duraiswami, R. & Prosperetti, A. 1992, 'Orthogonal mapping in two dimensions', *J. Comput. Physics* **98**, 254-268.
46. Kang, I.S. & Leal, L.G. 1992, 'Orthogonal grid generation in a 2D domain via the boundary integral method,' *J. Comput. Phys*. **102**, 78-87.
47. Blanco, A. & Magnaudet, J. 1995, 'The structure of the axisymmetric high Reynolds number flow around an ellipsoidal bubble of fixed shape,' *Phys. Fluids* **7**(6), 1265-1274.

48. Dandy, D.S. & Leal, G.L. 1986, 'Boundary layer separation from a smooth slip surface,' *Phys. Fluids* **29**, 1360-.
49. Kistler S.F. & Scriven L.E. 1983, 'Coating flows", Computational analysis of polymer processing,' Ed. J.R.A. Pearson and S. M. Richardson (Applied Science Publishers, London, 1983), p. 393.
50. Foteinopoulou, K., Mavrantzas, V.G. & Tsamopoulos, J. 2004, 'Numerical simulation of bubble growth in Newtonian and viscoelastic filaments undergoing stretching,' *J. Non-Newtonian Fluid Mech.* **122**, 177-200.
51. Salzman, J. & Brackbill, J. 1982, 'Applications and generalizations of variational methods for generating adaptive meshes', *Numerical Grid Generation*, Elsevier Sci, Publ., 865-884.
52. Christodoulou, K.N. & Scriven, L.E. 1992, 'Discretization of Free Surface Flows and Other Moving Boundary Problems,' *J. Comput. Phys*. **99**, 39-55.
53. Tsiveriotis, K. & Brown, R.A. 1992, 'Boundary-conforming mapping applied to computations of highly deformed solidification interfaces,' *Int. J. Num. Meth Fluids* **14**, 981-1003.
54. Dimakopoulos, Y. & Tsamopoulos, J. 2003, 'A quasi-elliptic transformation for moving boundary problems with large anisotropic transformations,' *J. Comput. Phys*. **192**, 494-522.
55. Puckett, E.G., 1991, 'A volume-of-fluid interface tracking algorithm with applications to computing shock wave refraction,' in proceedings 4th International Symposium on Computational Fluid Dynamics, Davis CA, edited by H. Dwyer, p. 933.
56. Brackbill, J.U., Kohe, D.B. & Zemack, C. 1992, 'A continuum method for modeling surface tension,' *J. Comput. Phys*. **100**, 335-354.
57. Sussman, M., Smereka, P. & Osher, S.J. 1994, 'A level set approach for computing solutions to incompressible two-phase flow,' *J. Comput. Phys*. **114**, 146-.
58. Blake, J.R., Taib, B.B. & Doherty, G. 1986, 'Transient cavities near boundaries. Part1. Rigid boundary,' *J. Fluid Mech*. **170**, 479-197.
59. Blake, J.R., Keen G.S., Tong, R.P & Wilson, M. 1999 'Acoustic cavitation: the fluid dynamics of non-spherical bubbles,' *Phil. Trans. R. Soc. Lond. A*. **357**, 251-267.
60. Philipp, A. & Lauterborn, W. 1998, 'Cavitation erosion by single laser-produced bubbles,' *J. Fluid Mech*. **361**, 75-116.
61. Popinet, S. & Zaleski, S. 2002, 'Bubble collapse near a solid boundary: a numerical study of the influence of viscosity,' *J. Fluid Mech*. **464**, 137-163.
62. Chahine G.L., Kalumuck, K.M. & Hsiao, C.T. 2003, 'Simulation of surface piercing body coupled response to underwater bubble dynamics utilizing 3DYNAFS, a three-dimensional BEM code,' *Computational Mechanics* **32**, 319-326.
63. Oguz, H.N. & Prosperetti, A. 1993, 'Dynamics of bubble-growth and detachment from a needle,' *J. Fluid Mech*. **257**, 111-145.
64. Liao, Y.C., Basaran, O.A. & Frances E.I. 2004, 'Hydrodynamic effects on the oscillations of supported bubbles: implications for accurate measurements of surface properties,' *Coll. & Surf. A: Physicochem. Eng. Aspects* **250**, 367-384.
65. Plesset, M.S. 1954, 'On the stability of fluid flows with spherical symmetry,' *J. Appl. Phys.* **25**(1), 96-98.
66. Brenner, M.P., Lohse, D. & Dupont, T.F. 1995, 'Bubble shape oscillations and the onset of sonoluminescence,' *Phys. Rev. Let*. **75**(5), 954-957.
67. Hall, P. & Seminara, G. 1980, 'Nonlinear oscillations of non-spherical cavitation bubbles in acoustic fields,' *J. Fluid Mech*. **101**, 423-444.
68. Longuet-Higgins, M.S. 1989, 'Monopole emission of sound by asymmetric bubble oscillations. Part 1. Normal modes,' *J. Fluid Mech*. **201**, 525-541.

69. J. Eggers, 1993, 'Universal pinching of 3D axisymmetric free surface flow,' *Phys. Rev. Lett*. **71,** 3458-3460.
70. Geisler, R. 2004, *Untersuchungen zur Laserinduzierten Kavitation mit Nanosekunden – Femtosekundenlasern*, Ph.D Thesis submitted to the University of Goettingen.
71. Tsiglifis, K. *Numerical simulations of the oscillations and collapse of bubbles and contrast agents* Ph.D Thesis to be submitted to the University of Thessaly.
72. Doinikov, A.A. & Zavtrak, S.T. 1995, 'On the mutual interaction of two gas bubbles in a sound field,' *Phys. Fluids* **7**(8), 1923-1930.
73. Ida, M. 2002, 'A characteristic frequency of two mutually interacting gas bubbles in an acoustic field,' *Phys. Let. A.* **297**, 210-217.
74. Ida, M. 2004, 'Investigation of transition frequencies of two acoustically coupled bubbles using a direct numerical simulation technique,' *J. Phys. Soc. Japan* **73**(11), 3026-3033.
75. Moore, D.W. 1965, 'The velocity of rise of distorted gas bubbles in a liquid of small viscosity,' *J. Fluid Mech.* **23**(4), 749-766.
76. Feng, & Z.C. Leal G.L. 1995 'Translational instabilities of a bubble undergoing shape oscillations,' *Phys. Fluids* **7**, 1325-1336.
77. Doinikov, A.A. 2004, 'Translational motion of a bubble undergoing shape oscillations,' *J. Fluid Mech*. **501**, 1-24.
78. Esmaeeli, A. & Tryggvason, G. 1999, 'Direct numerical simulations of bubble flows. Part 2: Moderate Reynolds Number Arrays,' *J. Fluid Mech*. **385**, 325-358.
79. Seta, T., Kono, K. & Chen, S. 2003, 'Lattice Boltzmann method for two-phase flows,' *Intern. J. of Mod. Phys. B* **17**(1&2) 169-172.
80. Bhaga, D. & Weber, M.E. 1981, 'Bubbles in viscous liquids: Shapes, wakes and velocities,' *J. Fluid Mech*. **105**, 61-85.
81. Blanco, A. 1995, *Quelques aspects de l'écoulement autour d'une bulle deformable: une approche par simulation directe*, PhD Thesis. Inst. Nat. Polytech. Toulouse, France.